

THE PENNSYLVANIA STATE UNIVERSITY  
SCHREYER HONORS COLLEGE

DEPARTMENT OF BIOMEDICAL ENGINEERING

STUDYING THROMBOSIS AND SURFACE ROUGHNESS IN THE PENN STATE  
PEDIATRIC VENTRICULAR ASSIST DEVICE

CECILIA A. RICHARDSEN  
SPRING 2019

A thesis  
submitted in partial fulfillment  
of the requirements  
for a baccalaureate degree  
in Biomedical Engineering  
with honors in Biomedical Engineering

Reviewed and approved\* by the following:

Keefe Manning  
Professor of Biomedical Engineering  
Thesis Supervisor

Justin Brown  
Professor of Biomedical Engineering  
Honors Adviser

\* Signatures are on file in the Schreyer Honors College.

## ABSTRACT

From 2010 to 2017, 439 children died while waiting for a donor heart among 4,731 children on the transplant list. (1) There is a clear shortage of hearts available for transplant and a need for a pediatric bridge-to-transplant device. To meet this need, the Division of Applied Biomedical Engineering at the Penn State College of Medicine has developed a pediatric ventricular assist device (PVAD). The Penn State PVAD is being tested currently in juvenile ovine models.

While animal studies have been encouraging, thrombus formation is observed, which is a major problem in ventricular assist devices. One hypothesis is that roughness on the surface of the segmented poly-(ether polyurethane urea) (SPEEU) seamless blood sac can lead to the aggregation of platelets in a fibrin matrix. These deposits can block blood flow through the device or become detached and migrate to another location. This can lead to device failure, heart attack, or stroke.

Explanted Penn State PVAD blood sacs from the ovine trials are examined to study surface irregularities in relation to the presence of platelet and fibrin deposits, which provides insight into why thrombosis occurs. Blood sacs are evaluated using immunofluorescent labeling and confocal microscopy. The samples are labeled with an indirect method using CAPP2A and Alexa Fluor 555 to label platelets and anti-fibrinogen and Alexa Fluor 488 to label fibrin. The sacs are viewed with confocal microscopy to determine if there are platelets or fibrin on the surface. The platelet and fibrin structures are confirmed by using environmental scanning electron microscopy (ESEM). The biological depositions are enzymatically degraded from the surface, and the sac surface roughness is studied with optical profilometry. The root mean squared ( $R_q$ ), an average deviation from the roughness average center line, roughness average ( $R_a$ ), an average of all values on the roughness profile, ten-point height ( $R_z$ ), an average of the five highest peaks and the five lowest

valleys, and Swedish height (H), a roughness average of the middle 90% of the data, are roughness parameters that are collected for each sample. Images taken from confocal, ESEM, and optical profilometry are correlated for each sample to determine the relationship between thrombus formation and surface topography.

For Rq, Ra, and H, the macroscopic regions are significantly rougher than the microscopic regions and control. The microscopic regions are significantly rougher than the control. For Rz, the macroscopic regions are significantly rougher than the control and the microscopic regions are significantly rougher than the control. Regions with greater deposition are correlated with higher values of roughness. Areas of higher surface roughness on the SPEUU seamless blood sacs could promote deposition of platelets and fibrin.

## TABLE OF CONTENTS

LIST OF FIGURES .....	iii
LIST OF TABLES .....	iv
ACKNOWLEDGEMENTS .....	v
Chapter 1 Introduction .....	1
1.1 Clinical Need .....	1
1.2 Mechanical Circulatory Support .....	2
1.3 Penn State Pediatric Ventricular Assist Device .....	6
1.4 Thrombosis and Material Properties .....	8
1.5 Recent Study .....	11
Chapter 2 Methods .....	13
2.1 Imaging and Analysis Techniques .....	13
2.1.1 Confocal Microscopy .....	13
2.1.2 Environmental Scanning Electron Microscopy .....	15
2.1.3 Optical Profilometry .....	17
2.2 Ovine Study at Penn State Hershey College of Medicine .....	21
2.3 Sample Preparation and Explanted Sac Analysis .....	22
2.3.1 Immunofluorescent Labeling and Confocal Microscopy .....	23
2.3.2 Environmental Scanning Electron Microscopy .....	26
2.3.3 Degradation of Biological Deposits .....	27
2.3.4 Optical Profilometry .....	27
Chapter 3 Results .....	30
3.1 Explanted Sac Analysis .....	30
3.1.1 Deposit Sizes by Location .....	31
3.1.2 Correlation of Confocal, ESEM, and Profilometry .....	35
3.2 Controls .....	44
3.3 Surface Roughness Analysis .....	46
Chapter 4 Discussion .....	51
4.1 Summary of Findings .....	51
4.1.1 Roughness Analysis .....	52
4.1.2 Macroscopic Deposits .....	53
4.1.3 Microscopic Deposits .....	53
4.2 <i>In Vivo</i> Study Correlation .....	54
4.3 Limitations and Future Studies .....	57
Additional Correlated Images of Macroscopic Deposits .....	59

Additional Correlated Images of Microscopic Deposits..... 71  
BIBLIOGRAPHY ..... 77

## LIST OF FIGURES

Figure 1. Example of extracorporeal membrane oxygenation (ECMO) in an infant patient, which is used as a heart-lung bypass system outside the body. (12).....	3
Figure 2. Example of the HeartMate II in an adult patient, shown with an external battery connecting to the heart pump via a percutaneous lead. (11).....	4
Figure 3. Various sizes of the Berlin Heart EXCOR VAD, which are used to accommodate different sized children. (15).....	5
Figure 4. Photograph of the Penn State Infant VAD, designed at the Penn State Hershey College of Medicine. (20) .....	7
Figure 5. Diagram of the factors released through different pathways of the coagulation cascade. (25).....	9
Figure 6. Diagram of the light path through a specimen for images captured by confocal microscopy. (35) .....	14
Figure 7. Sample confocal microscopy image taken of a biological deposit on the surface of Penn State PVAD Sac 223.....	14
Figure 8. Diagram of the electron beam, sample, and energy detection that generates images by environmental scanning electron microscopy. (36).....	16
Figure 9. Sample environmental scanning electron microscopy image taken of a biological deposit on the surface of Penn State PVAD Sac 183.....	16
Figure 10. Diagram of the light path through a specimen for images captured by optical profilometry. (38).....	17
Figure 11. Graph of the roughness average calculated along the sampling length of a material. (40).....	18
Figure 12. Comparison of the roughness average (Ra) and the root-mean-square roughness (Rq). (40).....	19
Figure 13. Graph of the ten-point-height calculated along the evaluation length of a material. (40).....	19
Figure 14. Graph of the Swedish height calculated along the sampling length of a material. (40).....	20
Figure 15. Calculation of surface roughness parameters (Rq [shown in this software as rms], Ra, Rz, and H) using MetroPro using data collected from a surface of a Penn State PVAD blood sac. Surface roughness parameters are highlighted in red. ....	21
Figure 16. Schematic of the locations on the blood sac. This diagram is used to describe the locations of deposits and for regions of sampling. ....	22
Figure 17. Sampling regions of blood contacting sac. Left: diaphragm side facing forward. Right: stationary side facing forward.....	23

Figure 18. Patterned method for imaging samples. Twelve regions are imaged for each sample. (35).....	23
Figure 19. Indirect immunofluorescent labeling method used for labeling.....	25
Figure 20. The MetroPro interface shows a piece of debris with elevated topography on the 3D model. This is an example of an area that would be masked and removed from surface analysis.....	28
Figure 21. An example of a profilometry image from Sac 249, Sample 4, Region 3 (A) without masking and (B) with masking applied. ....	29
Figure 22. Correlation of (A) confocal, (B) ESEM, and (C) profilometry images on the inlet of Sac 170. There is a small microscopic deposit circled in red and a scratch shown by the arrows.....	35
Figure 23. Correlation of (A) confocal, (B) ESEM, and (C) profilometry images on the inlet top of Sac 172. There is a small microscopic deposit circled in red. ....	36
Figure 24. Correlation of (A) confocal, (B) ESEM, and (C) profilometry images on the outlet top of Sac 183. There is large macroscopic deposition shown within the red boxes. Topography shows some residual biologics.....	38
Figure 25. Correlation of (A) confocal, (B) ESEM, and (C) profilometry of the inlet top of Sac 190. There is scatted deposition circled in red. The arrows point to a scratch on the surface.....	39
Figure 26. Correlation of (A) confocal, (B) ESEM, and (C) profilometry of the outlet top of Sac 190. Scattered deposition is shown by the red arrows and spreads across regions 11 and 12.....	40
Figure 27. Correlation of (A) confocal, (B) ESEM, and (C) profilometry on the inlet bottom of Sac 223. There is a large macroscopic deposit seen on the surface. The biologics were not fully degraded from the profilometry image.....	40
Figure 28. MetroPro analysis for region 5 of the inlet bottom on Sac 223. The 3D model and surface profile show the raised topography in the area of interest. ....	41
Figure 29. Correlation of (A) confocal, (B) ESEM, and (C) profilometry on the outlet top of Sac 223. There is a small, macroscopic deposit shown in the red circles. ....	41
Figure 30. Correlation of (A) confocal, (B) ESEM, and (C) profilometry on the outlet bottom of Sac 234. There was a small, microscopic deposit shown by the red circles.....	42
Figure 31. Correlation of (A) confocal, (B) ESEM, and (C) profilometry on the outlet of Sac 240. There is a microscopic deposit shown by the red circles.....	43
Figure 32. Correlation of (A) confocal, (B) ESEM, and (C) profilometry on the bottom of Sa 240. There is a moderate microscopic deposit on region 4 and a small microscopic deposit on region 11 shown by the red circles. There is a scratch on region 4 that is shown by the red arrows.....	43

Figure 33. Correlation of (A) confocal, (B) ESEM, and (C) profilometry on the inlet top of Sac 240. There is a small microscopic deposit shown by the red circles. ....	44
Figure 34. Correlation of (A) confocal, (B) ESEM, and (C) profilometry on the outlet top of Sac 240. There is a microscopic deposit shown by the red circles. ....	44
Figure 35. Images taken by confocal (A) and ESEM (B) of the control sac. No fluorescence is noted. ....	45
Figure 36. Map of all deposits for the 13 sacs analyzed. ....	48
Figure 37. Comparing average Rq, Ra, and H values between macroscopic and microscopic deposits and a control sac. Error bars indicate the standard error of the mean. ....	49
Figure 38. Comparing average Rz values between macroscopic and microscopic deposits and a control sac. Error bars indicate the standard error of the mean. ....	50
Figure 39. A small, macroscopic deposit found with (A) confocal, was confirmed with (B) ESEM at the inlet of Sac 170. The (C) profilometry showed scuffing. (34).....	60
Figure 40. A closer examination of (A) Region 8 and (B) Region 9 of the inlet of Sac 170. (34)	61
Figure 41. A large, macroscopic deposit found with (A) confocal and confirmed with (B) ESEM. Residual biologics are seen on (C) the profilometry of the inlet of Sac 183. (34) .....	62
Figure 42. A closer examination of (A) Region 7 and (B) Region 8 of the inlet of Sac 183. (34)	63
Figure 43. A very large macroscopic deposit seen by (A) confocal and (B) ESEM on the outlet of Sac 183. The (C) profilometry shows residual biologics on the surface. (34).....	64
Figure 44. A closer examination of (A) Region 2 and (B) Region 6 of the outlet of Sac 183. (34)	65
Figure 45. A large, macroscopic deposit shown by (A) confocal and (B) ESEM. There are residual biologics on (C) the profilometry image of the outlet of Sac 190. (34) .....	67
Figure 46. A closer examination of (A) Region 7 and (B) Region 11 of the outlet of Sac 190. (34)	68
Figure 47. A dense, macroscopic deposit shown by (A) confocal and (B) ESEM. The (C) profilometry shows residual biologics on the outlet of Sac 234. (34) .....	69
Figure 48. A closer examination of (A) Region 9 and (B) Region 11 of the outlet of Sac 234. (34)	70
Figure 49. Small deposits found on confocal and ESEM with the topography showing a scuffed surface on the center front of Sac 170. (A) Region 7 and (B) Region 8 are highlighted. (34)	71
Figure 50. A small deposit shown by confocal and ESEM at Region 5 on the inlet side of Sac 172. The profilometry image shows debris on the surface. (34) .....	72
Figure 51. A small deposit shown by confocal and ESEM on Region 2 of the inlet of Sac 176. The profilometry shows a smooth surface. (34) .....	72

- Figure 52. A large, microscopic deposit was shown by confocal and ESEM on Regions 5 and 6 of the outlet side of Sac 183. The profilometry shows residual biologics. (34)..... 73
- Figure 53. Yellow, microscopic deposits are shown by confocal and confirmed by ESEM on Region 6 of the center back of Sac 190. The profilometry shows some scuffing on the topography. (34)..... 73
- Figure 54. Red deposits are shown by confocal and seen faintly with ESEM on Region 11 of the center back of Sac 192. The topography shows some debris or pitting. (34) ..... 74
- Figure 55. Large, microscopic deposits are shown on confocal and seen faintly on ESEM in Regions 3 and 11 of the top sample of Sac 223. A rougher surface is observed from the profilometry images. (34) ..... 74
- Figure 56. A small, microscopic deposit shown on confocal and confirmed with ESEM on Region of the outlet of Sac 232. The profilometry shows a smooth surface. (34) ..... 75
- Figure 57. A deposit shown by confocal and confirmed by ESEM on Region 5 of the center front of Sac 234. The red arrow points to a scratch shown on the profilometry image. (34) ... 75
- Figure 58. Red deposits shown by confocal and ESEM on Regions 10 and 12 of the top sample of Sac 247. A divot is shown on the ESEM and profilometry of Region 12. (34) ..... 76
- Figure 59. A small, green deposit is shown on confocal and confirmed with ESEM. The red arrow points to debris on the topography of the profilometry image. (34) ..... 76

**LIST OF TABLES**

Table 1. Deposits at Location 1: Inlet.....	31
Table 2. Deposits at Location 2: Outlet .....	31
Table 3. Deposits at Location 3: Center Front.....	31
Table 4. Deposits at Location 4: Center Back .....	32
Table 5. Deposits at Location 5: Top.....	32
Table 6. Deposits at Location 6: Bottom.....	32
Table 7. Deposits at Location 7: Inlet Side.....	33
Table 8. Deposits at Location 8: Outlet Side .....	33
Table 9. Deposits at Location 9: Inlet Bottom.....	33
Table 10. Deposits at Location 10: Outlet Bottom .....	34
Table 11. Deposits at Location 11: Inlet Top .....	34
Table 12. Deposits at Location 12: Outlet Top.....	34
Table 13. Summary of Roughness Data for Macroscopic Deposits .....	46
Table 14. Summary of Roughness Data for Microscopic Deposits.....	47
Table 15. Animal Study Statistics from the Penn State Hershey Medical Center. Macroscopic deposit locations are highlighted. ....	55
Table 16. Qualitative Summary of Animal Studies from the Penn State Hershey Medical Center. Macroscopic deposit locations are highlighted. ....	56

## ACKNOWLEDGEMENTS

I would like to first express my sincere gratitude Dr. Keefe Manning for serving as my thesis advisor and as an excellent mentor. He has offered me many opportunities to grow as a researcher and has challenged me to become a more critical thinker. I am deeply thankful for his guidance and feedback throughout this entire project.

I am thankful for Dr. Justin Brown and Dr. William Weiss for their participation on my thesis committee. I would also like to thank Branka Lukic for her kindness and willingness to answer all of my questions about the animal studies. The Division of Applied Biomedical Engineering at the Penn State Hershey College of Medicine have provided me with exceptional opportunities to learn and I am grateful for all of their efforts.

Thank you to Ashlyn Mueser for introducing me to this protocol and for contributing extensive work to this project. In addition, this project would not have been possible without funding from American Heart Association Grant 18UFEL33900164, and NIH grants HL108123 and HL131921.

I am thankful for the members of the Artificial Heart Lab and for the times we have shared during summertime lab cleanup, trivia night, and of course the pursuit of different topics within the field of cardiovascular fluid dynamics research. A helping hand or a listening ear was never far away in this lab group. I would also like to acknowledge Ashley Nguyen for her eagerness to learn the explanted sac protocol and wish her much success with her future research. A very special thanks goes to Katie Blankemeyer, Clare McHugh, and Cara Pearson for constantly making me laugh and for being with me every step of the way. I am certainly blessed by fantastic friends and family members who have provided an incredibly strong support network over the past four years. It has been a wonderful journey.

## **Chapter 1**

### **Introduction**

#### **1.1 Clinical Need**

Cardiovascular disease (CVD) remains the leading cause of death globally, contributing to 17.7 million, or 31%, of total deaths in 2017. (2) In the United States alone, it is estimated that 92.1 million adults were living with at least one type of CVD in 2017. CVD includes a variety of conditions, such as heart disease, heart attack, stroke, heart failure, arrhythmia, and heart valve disease. (3) While some forms of CVD can be treated with lifestyle changes or medications, there are times when surgical intervention is necessary. For patients who have had little success with medications or minor procedures, a heart transplant can be performed to replace the diseased, failing heart with a more functional donor heart. Advances in technology and modifications to surgical procedure have improved the 1-year survival rate following heart transplantation from about 30% in 1970 to about 90% in 2017. (4) From 1987 to 2012, there were 40,253 adults waiting for heart transplants and only 26,943 transplants were performed. (3) Despite the improvement in 1-year survival rate, there is a shortage of donor hearts available, making heart transplantation an unsustainable solution.

While this is clearly a prevalent issue for adults, treatments for CVD in children also remain problematic. In pediatric patients, the most common forms of CVD are congenital heart disease and cardiomyopathy, both of which usually result in fatal outcomes. As of 2016, it was estimated that 1 in every 40,000 births is affected by congenital heart failure. (5) Pediatric cardiomyopathies are expected to occur 1.3 times in every 100,000 births. (6) The therapy of choice for end stage heart failure in children is heart transplantation, due to the higher survival rates, quality of life, and

fewer adverse effects compared to other treatment options. (7) From 2010 to 2017, 439 children, among the 4,731 children on the transplant list, died while waiting to receive a donor heart. (8) Considering the prevalence of CVD, the shortage of viable donor hearts, and the current lack of effective therapy for patients with end-stage heart failure, alternative treatment options are necessary.

## **1.2 Mechanical Circulatory Support**

Mechanical circulatory support is an intervention that can extend life by serving as a bridge-to-transplant. A ventricular assist device (VAD), the most common form of mechanical circulatory support, is an implantable device that helps blood pump out of the ventricles. VADs can be implanted on the right, left, or both sides of the heart, but are most commonly required on the left side to support the high demands of pumping blood to the entire body. Research on the development of these support devices began in the 1960s, and the first left ventricular assist device (LVAD) was approved by the FDA in 1994 as a bridge-to-transplant. (9) Today, LVADs are additionally used for bridge-to-recovery or destination therapy. Technological advancements in the last 25 years have led to VADs that have increased durability and smaller size, with some devices being completely implantable. (10) LVADs have become a widely accepted form of treatment for adults with heart failure in the situation that transplantation is not feasible. However, mechanical circulatory support has found limited success in pediatric cases.

The original method of mechanical support for children was extracorporeal membrane oxygenation (ECMO), which was designed as a cardiopulmonary bypass that supports life in patients suffering from respiratory failure and circulatory complications. ECMO is used primarily

as a form a rescue therapy, and has maintained mortality rates between 40-50% over the past several decades. A diagram detailing the setup of ECMO treatment is shown in Figure 1. The technology provides benefit over not providing any surgical intervention, but it is not a long-term solution. ECMO has led to numerous complications, including bleeding, blood clotting, infection, and inadequate oxygen delivery to the body. (12) Based on these complications and the high mortality rate, other mechanical support options have been explored for pediatric patients.

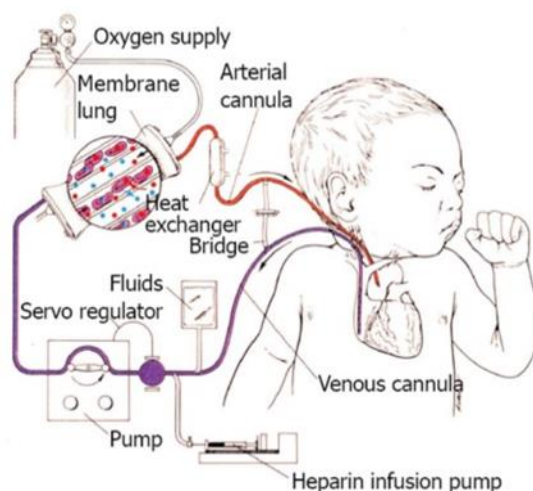


**Figure 1. Example of extracorporeal membrane oxygenation (ECMO) in an infant patient, which is used as a heart-lung bypass system outside the body. (12)**

The adult-sized LVADs have been considered for pediatric patients, but have seen limited application in infants and small children due to size constraints. An example of an LVAD is shown in Figure 2. A study in 2011 testing the efficacy of the HeartMate II LVAD in 28 patients ages 11-18 years old showed 90% of patients had received a transplant or reached recovery at a 6 month follow up. (13) The HeartWare HVAD is slightly smaller in size compared to the HeartMate II and was tested in 13 children ages 3 to 10 years old in 2015. The study showed that 11 of the 13 patients survived to transplant or recovery, while 4 of the 13 patients had pump thrombosis, which

was a much higher proportion when compared with a study on young adults. (14) While some LVAD studies have been successful in young adults, there is a need for an ECMO alternative for small children and a solution to minimize complications like bleeding, thrombosis, and infection.

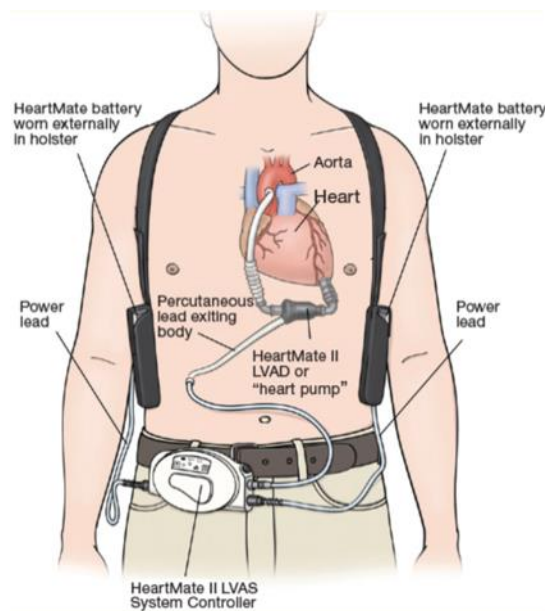


**Figure 2. Example of the HeartMate II in an adult patient, shown with an external battery connecting to the heart pump via a percutaneous lead. (11)**

This need has led to the development of VADs specifically for the pediatric population, known as pediatric ventricular assist devices (PVADs). The only PVAD currently approved by the FDA is the Berlin Heart EXCOR VAD, which was first implanted in a pediatric patient in 2000. The system consists of one or two extracorporeal pneumatically driven blood pumps. The pulsatile device is available in a variety of sizes, as shown in Figure 3, to accommodate children in different stages of physical development. (15) The Berlin Heart EXCOR Investigational Device Exemption Trial (IDE) between 2007 and 2010 demonstrated a transplant or recovery rate of 70.6% among all patients, ranging from 6 days to 4 years old. Adverse events occurred in more than 25% of patients, with the most common effects being major infection, bleeding, hypertension, and

neurological dysfunction. Two-thirds of patients weighing <5kg died while on Berlin EXCOR support. (16)



**Figure 3. Various sizes of the Berlin Heart EXCOR VAD, which are used to accommodate different sized children. (15)**

Other PVADs currently in development are the HeartMate 3, the HeartWare MVAD, the Jarvik Infant VAD, and the Penn State PVAD. (15) The HeartMate 3 uses a centrifugal pump and features a magnetically levitated rotor. This device is a miniaturized intrapericardial continuous-flow pump. One clinical trial resulted in a 30-day survival for 49 out of 50 adult patients, and a 6-month survival for 46 out of 50 patients with no pump thrombosis events. The most common adverse effects were bleeding, arrhythmia, and infection. (17) The HeartWare MVAD is a miniaturized ventricular assist device that features a 22 mL displacement volume and a continuous-flow pump. This device was designed to limit surgical invasiveness by reducing the size of the pump housing and by providing an adjustable inflow cannula depth. The HeartWare MVAD underwent an ovine trial with a target study duration of 90 days. The trial reported that 7 of the 9 animals survived for at least 90 days, with no device malfunctions or macroscopic evidence of mechanical wear. Trials are continuing for the HeartMate 3 and the HeartWare MVAD, with both devices showing potential for pediatric application. (18) The Jarvik Infant VAD is an intracorporeal, axial-flow device designed specifically for neonates and infants. The infant pump

has a 4 mL displacement volume and is based on the Jarvik 2000 model, but with different blade design to accommodate to the pediatric anatomy. This device was tested in a neonate piglet model for 6 hours and the trial reported no thrombosis events. (19) However, a major limitation of the trial is the short-term study, showing a need for the device to be tested for a longer period of time. A new iteration of this model, the Jarvik Infant 2015, is undergoing pre-clinical testing. (15)

These devices are created to be small so they can appropriately match the size of the device to the size of the patient. They are also designed to reduce risk of infection and minimize thrombosis. While significant strides have been made in the area of PVAD development over the past two decades, further testing and progress is necessary to provide effective therapy for pediatric cases of heart failure.

### **1.3 Penn State Pediatric Ventricular Assist Device**

The Division of Artificial Organs at the Penn State College of Medicine has developed a PVAD to meet the need of a pediatric bridge-to-transplant. The major focus of the project has been to scale a VAD down to pediatric or infant size while minimizing thrombus formation. Figure 4 shows the Penn State PVAD, which was based on an adult model, the Pierce-Donachy VAD, and is a pneumatically driven, pulsatile pump that was designed for paracorporeal placement. (20)



**Figure 4. Photograph of the Penn State Infant VAD, designed at the Penn State Hershey College of Medicine. (20)**

The device features 17 mm Björk-Shiley Monostrut Delrin disk valves that are custom fit to the pump. These valves promote high velocities of blood entering the pump, creating high wall shear rates, which contributes to the washing of the surface and the reduction of recirculation, thus decreasing the likelihood of thrombus formation. (20) Another key feature of the device is the seamless segmented polyether polyurethaneurea (SPEUU) blood sac, which is positioned within a titanium case, mechanical heart valves, and cannula connectors. The seamless design reduces irregularities along the blood contacting surface. (21) There is evidence that surface irregularities can cause platelet activation and lead to thrombus formation, so the seamless blood sac and the close tolerances in mating parts function to reduce thrombosis due to small imperfections along the blood contacting surface. (22)

The Penn State PVAD recently completed a series of chronic *in vivo* ovine trials. Juvenile sheep (20-25 kg) were chosen for the study due to their size, anatomy, thrombogenicity, and hemodynamics, among other factors. The intended duration of each study was 4-6 weeks. The survival time ranged from 5 to 41 days, with a mean survival rate of 26.1 days. (23) Anticoagulation was given in two different groups. One group received heparin to reach a target

activated partial thromboplastin (aPTT) time of 1.5-2 times the normal value. The second group received heparin to reach a target thromboelastography (TEG) R-time of 2 times the normal. The second group required lower levels of heparin. Following each study, the PVAD was explanted and thromboembolism was searched for in each animal. The blood contacting surfaces of the pumps were analyzed for thrombus formation. Minimal thrombosis was observed, even in the group that received lower levels of heparin. (24) While the trials were successful in minimizing thrombus formation, further improvements can still be made.

#### **1.4 Thrombosis and Material Properties**

Thrombosis is the coagulation of blood in the circulatory system. The formation of blood clots creates a significant risk of embolism, should the clot detach and become lodged somewhere further down the blood stream, effectively blocking blood flow. Adverse effects caused by embolism include heart attack, stroke, deep vein thrombosis, and pulmonary embolism. There is a higher risk of thrombosis upon implanting mechanical circulatory support devices because performing surgery and introducing blood contacting biomaterials to the body are factors that can trigger the coagulation cascade.

Blood coagulates as a mechanism to stop bleeding and protect the body against injury. This process is initiated when a vessel breaks and releases collagen, which releases factors that attract platelets to the wound site. Platelets are small, disc-shaped that can be activated mechanically or chemically. An activated platelet can activate other platelets and catalyze the coagulation cascade. The platelets can become active when in contact with adhesion proteins such as collagen, thrombin, or von Willebrand factor. These proteins trigger activation by interacting with platelet

surface receptors, causing the platelet to release cofactors that contribute to the coagulation cascade and increase the production of thrombin. Following the coagulation pathway, as shown in Figure 5, soluble fibrin is activated when thrombin comes in contact with fibrinogen. This results in the formation of a fibrin matrix, which traps red blood cells and platelets, effectively forming a blood clot. This coagulation pathway can also be initiated when a foreign material enters the body, which can occur as a result of the implantation of ventricular assist devices, making the reduction of thrombosis necessary. (24)

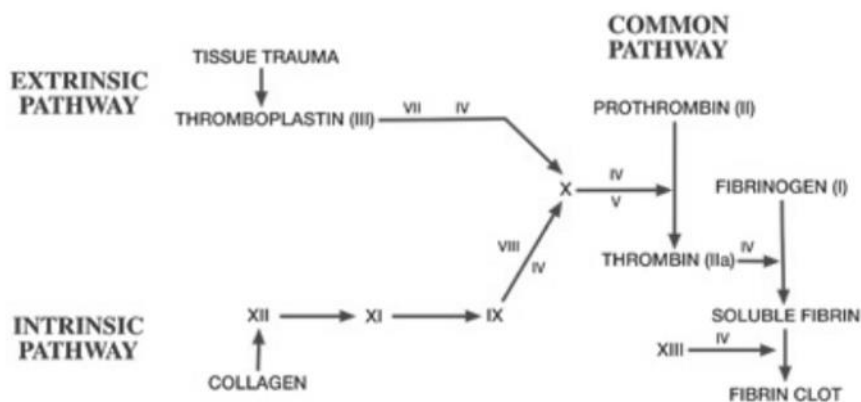


**Figure 5. Diagram of the factors released through different pathways of the coagulation cascade. (25)**

Anticoagulation therapy can function to disrupt the natural clotting process and protect against thrombosis in mechanical support devices. The two most common treatments are heparin and warfarin. While these interventions have been effectively used for adults, children respond differently to anticoagulation therapy, creating challenges for the implantation of VADs in pediatric patients. (26)

Another challenge for the prevention of thrombosis is choosing materials with high hemocompatibility, which describes how the body responds when a biomaterial is in contact with

blood. Material selection in cardiovascular devices is critical because there is evidence that surface irregularities on blood contacting surfaces can induce platelet adhesion, thereby triggering the coagulation cascade. Polyurethane is one of the most common materials used for the production of blood contacting devices because of its desirable qualities including high chemical resistance and tensile strength. Segmented polyurethane in particular is tough, durable, and flexible, making it useful in cardiovascular devices. (27) SPEUU, a type of segmented polyurethane, is currently being used in the Penn State PVAD to make the blood sacs. The method for developing the blood sacs began originally as a wax cast dipped into polydimethylsiloxane (PDMS) and then the wax cast was melted and cracked to remove the sac from the mold. Studies by Yamanaka *et al.* showed that scratch marks and pits were present on the surface of the blood sacs following the wax casting method. The current fabrication method uses a stainless steel mandrel instead of the wax mold. (28) While the seamless SPEUU design is believed to reduce pits on the surface of the blood sac, further investigation is necessary to understand if this material successfully minimizes platelet adhesion and thrombus formation.

A study by Milner *et al.* investigated the relationship between sub-micron textures and platelet adhesion on polyurethane biomaterials. While surface irregularities can induce platelet adhesion, this study showed that sub-micron irregularities were able to reduce platelet adhesion. To test the phenomenon, textured polyurethane was adhered to a rotating disk where the material spun in platelet rich plasma and compared to smooth, un-texturized samples. The results showed that the sub-micron textures were observed to reduce platelet adhesion at low shear stresses between 0 and 5 dyn/cm<sup>2</sup>. (29) These methods have yet to be tested in a pulsatile VAD. In another study by Hubbell and McIntire, epifluorescent video microscopy was used to visualize cell and surface interactions for collagen, polyurethane, and nylon surfaces. The study monitored

thrombosis at shear rates of  $100 \text{ s}^{-1}$  and  $500 \text{ s}^{-1}$ . At the lower shear rate, platelets coagulated on polyurethane and quickly embolized. At the higher shear rate, the platelets were not able to form bonds to the surface of the polyurethane. (30) Understanding the interactions of platelets with blood-contacting biomaterials is vital to the development of mechanical circulatory support devices. There are multiple factors that have been found to influence blood compatibility and thrombosis in VADs. A study at the University of Pittsburgh considered different hemodynamic conditions and hemostatic alterations in relation to thrombosis and thromboembolism. (31) Results indicated that regions of low flow had the highest incidence of thrombotic deposition during *in vitro* testing and platelet activation was elevated during the preoperative and implantation periods of clinical VAD use. Platelet deposition was evaluated *in vitro* with fluorescence microscopic observation. Future studies may further characterize the impact of mechanical parts involved in VAD design, incorporate cellular surfaces on blood contacting materials to possibly reduce adverse platelet adhesion, and improve the quality of numerical fluid dynamic assessment. While there are numerous studies on platelets and biomaterials as related to mechanical circulatory support, further understanding remains necessary.

### **1.5 Recent Study**

A study by Yamanaka investigated thrombus formation on the blood-contacting surfaces of polyurethane-urea blood sacs implanted in calves. Microscopic evaluation of the topography of the surface of the material revealed that biological deposits were found in regions of rough topography, suggesting that surface roughness may have a correlation with platelet adhesion. (28) Similar studies have also provided evidence that there may be a relationship between thrombosis

and surface topography of blood-contacting materials (29, 32) demonstrating a need to study the implications of this relationship as related to the Penn State PVAD. A protocol was developed to correlate different imaging techniques in order to understand the correlation between thrombus formation and surface topography in the SPEUU blood sacs of the Penn State PVAD. (33)

This protocol was used to analyze 11 of the ovine trials. (34) The project has been continued through analysis of 2 more ovine trials, including sampling more regions on the original 11 trials. Samples from blood sacs are prepared with an immunofluorescent labeling protocol that uses various antibodies to target platelets and fibrin. The stained samples are imaged with confocal microscopy to determine if there is any thrombosis on the surface and where the deposits are located. The samples are further imaged with environmental scanning electron microscopy (ESEM) in low vacuum mode to verify the structures of the deposits observed with confocal. The biological depositions are enzymatically degraded from the surface to get a better understanding of the true surface of the material. The surface of the blood sac is imaged with optical profilometry to obtain roughness parameters including roughness average, root-mean-square, Swedish height, and ten-point-height. A patterned method is used for each imaging technique so that a regional correlation can be performed between thrombus formation and surface roughness. Based on previous studies, it is expected that regions of increased roughness will be correlated with increased prevalence of deposition on the surface of the blood sac.

## **Chapter 2**

### **Methods**

#### **2.1 Imaging and Analysis Techniques**

Several imaging techniques were used to identify and verify the thrombotic structures on the surface of the blood sacs and to understand the surface roughness of the material. Confocal microscopy was used to locate fluorescent platelets and fibrin. Environmental scanning electron microscopy (ESEM) was used to verify the structures of platelets and fibrin. Optical profilometry was used to analyze the surface roughness of the blood sac once biologics were degraded from the surface. These three techniques were correlated to relate thrombosis to surface roughness.

##### **2.1.1 Confocal Microscopy**

Confocal microscopy (Olympus America Inc., Center Valley, Pennsylvania) uses spatial filtering to capture focused, high-quality images of fixed or living specimens. The microscope emits light from a laser system and through a pinhole aperture. The light is reflected and scanned across the specimen, and the fluorescence emitted from the specimen in the focused plane is passed to the detector. The objective in the confocal microscope can be adjusted to focus on different planes of the specimen. An advantage of this imaging technique is its ability to image thin sections of specimens that have a thickness of 50 micrometers or more. By focusing on thin planes and reducing background fluorescence, contrast and definition of the images are improved. Confocal microscopy also offers a zoom feature that allows the magnification to be altered without adjusting the objectives. The main disadvantage is that the microscope only offers limited excitation

wavelengths, in comparison to widefield microscopes that offer a full range of wavelengths. The high-intensity laser emission can also be damaging to living cells and tissues. (35) A diagram of the light path is shown in Figure 6. A sample image taken from confocal microscopy during this study is shown in Figure 7.

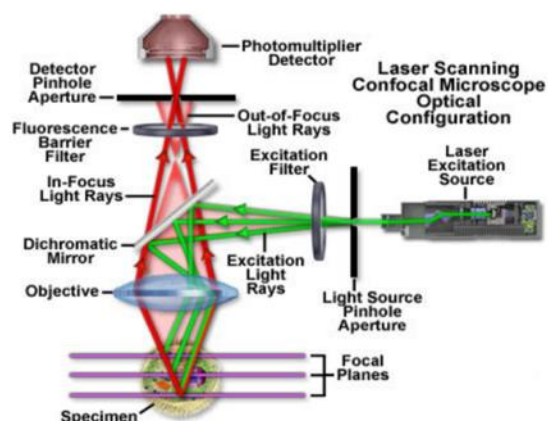


**Figure 6. Diagram of the light path through a specimen for images captured by confocal microscopy. (35)**

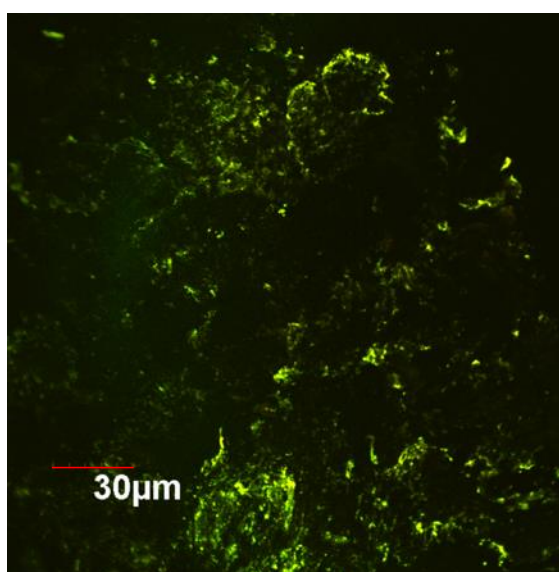


**Figure 7. Sample confocal microscopy image taken of a biological deposit on the surface of Penn State PVAD Sac 223.**

### **2.1.2 Environmental Scanning Electron Microscopy**

ESEM (FEI, Hillsboro, Oregon) is an imaging technique where the surface of the specimen is excited by a beam of electrons. When the beam of electrons strikes the sample, secondary and backscattered electrons are emitted due to inelastic and elastic collisions of the electron beam with the sample, respectively. The energy released from these collisions is detected by the instrument so that the images can be visualized. (37) Environmental scanning electron microscopy is different from conventional scanning electron microscopy because it allows uncoated specimens to be imaged in a high pressure chamber of water vapor. A diagram of the ESEM process is shown in Figure 8. (36)

The main advantage of this technique is that wet and insulating samples can be imaged without preparation by sputter coating. Specimens can be destroyed by the preparation methods required for conventional SEM, so ESEM offers a useful alternative for capturing images of a variety of biological materials. A disadvantage of ESEM is that the electron beam can undergo large-angle collisions, exciting regions outside the area of interest and reducing image contrast. While the resolution of ESEM images is not as high as conventional SEM, quality images are still possible because the water vapor in the chamber hydrates the sample and dissipates the build-up of charge generated by the electron beam. (37) A sample image taken from ESEM during this study is shown in Figure 9.

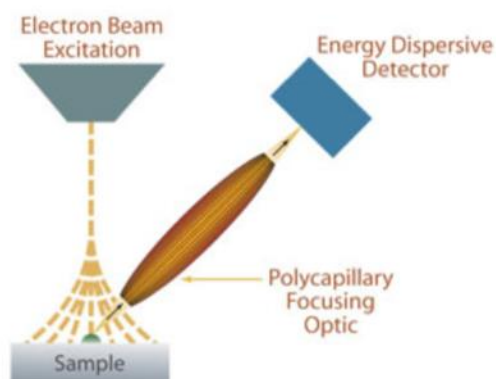


Figure 8. Diagram of the electron beam, sample, and energy detection that generates images by environmental scanning electron microscopy. (36)

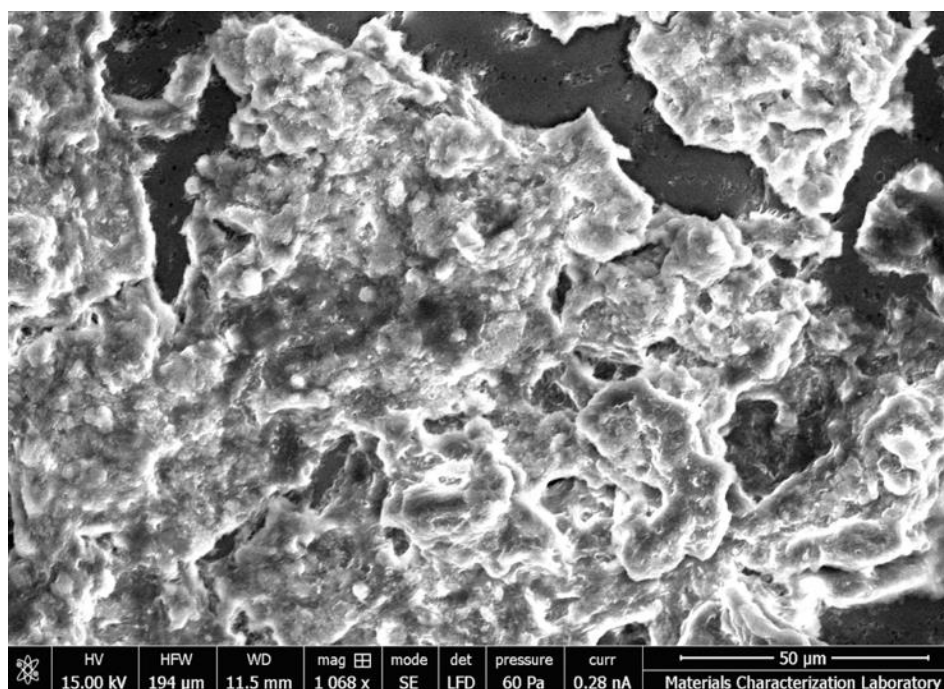
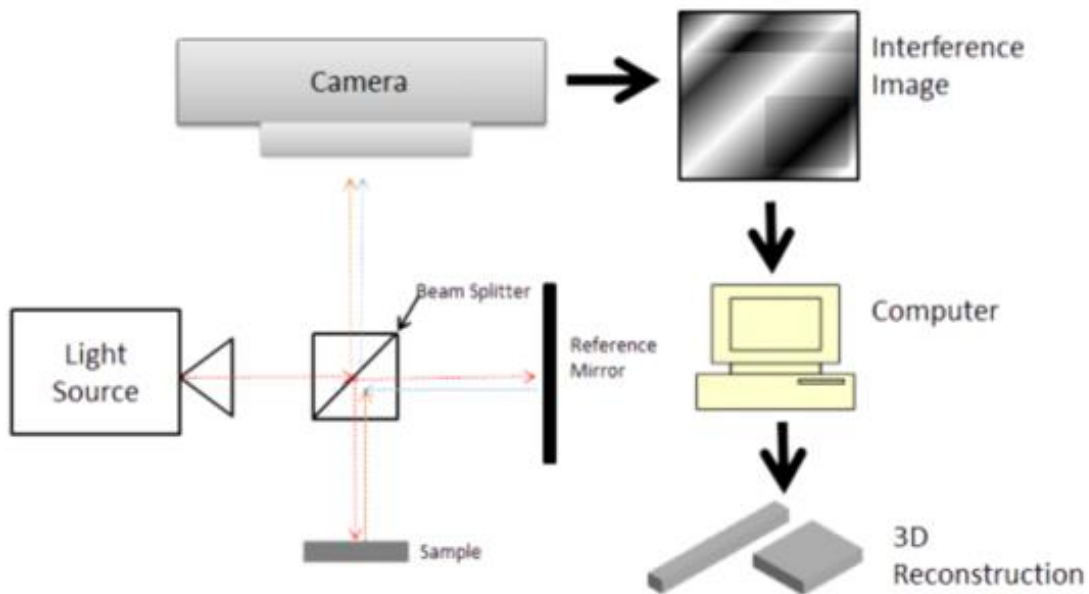


Figure 9. Sample environmental scanning electron microscopy image taken of a biological deposit on the surface of Penn State PVAD Sac 183.

### 2.1.3 Optical Profilometry

Optical profilometry is used to obtain data about the topography of a surface without contacting the sample. This imaging technique can be used to measure roughness, step height, shape, and thickness of surfaces. When light is emitted from the source, the beam is split into two parts. One part of the beam is passed through the test material, and the other part of the beam is reflected on a mirror. The divided beams are recombined and passed to the camera, which processes data regarding the topography of the surface. (39) A schematic of this process is shown in Figure 10. (38)



**Figure 10. Diagram of the light path through a specimen for images captured by optical profilometry. (38)**

The data collected from optical profilometry can be quantitatively analyzed with the MetroPro software. Roughness parameters used include the roughness average,  $R_a$ , the root-mean-square roughness,  $R_q$ , the ten-point-height,  $R_z$ , and the Swedish height,  $H$ .

The roughness average is the arithmetic average of the absolute values of the roughness profile. The calculation is given by Equation 1, where  $L$  is the length of the sample and  $z(x)$  is the profile of the surface. (40) Figure 11 provides a graphical example of the  $R_a$ , where each point of the profile is averaged to obtain the center line.

$$R_a = \frac{1}{L} \int_0^L |z(x)| dx \quad (1)$$

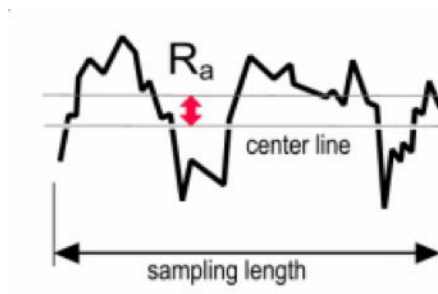


**Figure 11. Graph of the roughness average calculated along the sampling length of a material. (40)**

The root-mean-square roughness ( $R_q$ ) is the average of the deviations measured from the roughness average center line. Equation 2 demonstrates the calculation of the  $R_q$ . (40) Figure 12 shows a comparison between the  $R_q$  and the  $R_a$ . The  $R_q$  is larger than the  $R_a$  because it is more sensitive to extreme peaks and valleys.

$$R_q = \sqrt{\frac{1}{L} \int_0^L z^2(x) dx} \quad (2)$$

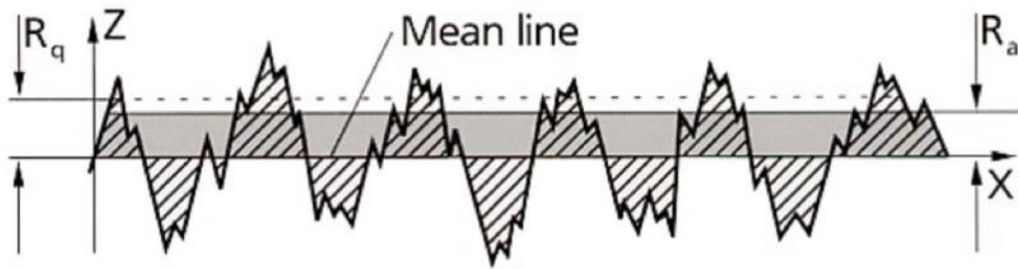


**Figure 12. Comparison of the roughness average (Ra) and the root-mean-square roughness (Rq). (40)**

The ten-point-height ( $R_z$ ) is the average of the five highest peaks and the five lowest valleys over the measured length of the material. Calculation of the  $R_z$  is shown in Equation 3.

(40) Figure 13 graphically shows how the peaks and valleys are compared to the average roughness of the surface.

$$R_z = \frac{(P1 + P2 \dots P5) - (V1 + V2 \dots V5)}{5} \quad (3)$$

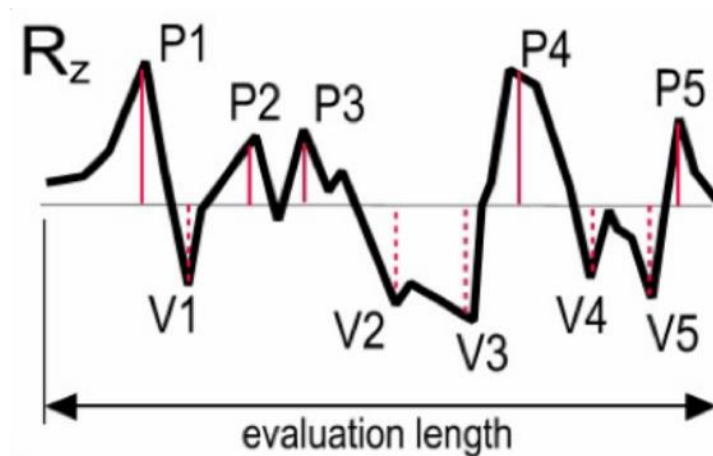


**Figure 13. Graph of the ten-point-height calculated along the evaluation length of a material. (40)**

The Swedish height (H) gives the roughness average of the middle 90% of the data. This parameter is less sensitive to the peaks and valleys. A graphical representation of the Swedish height is given in Figure 14, showing 5% of the data above the upper reference line and 5% of the data below the lower reference line. (40)

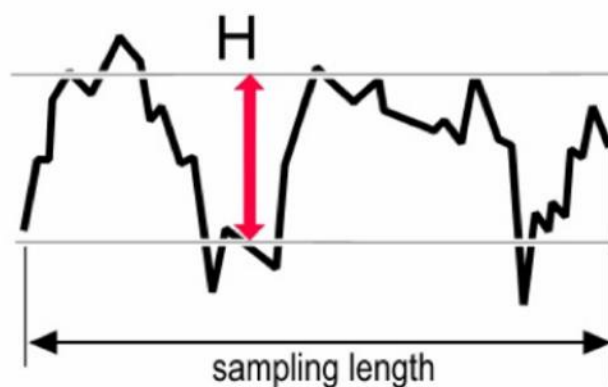


**Figure 14. Graph of the Swedish height calculated along the sampling length of a material. (40)**

MetroPro® 8.3.5 is a software that provides quantitative data for surface texture parameters from optical profilometry data. The profilometer has sub-angstrom resolution, so the quantitative roughness data were measured in nanometers and taken to one decimal place. An example of the MetroPro user interface is shown in Figure 15, with the desired roughness parameters outlined in red.

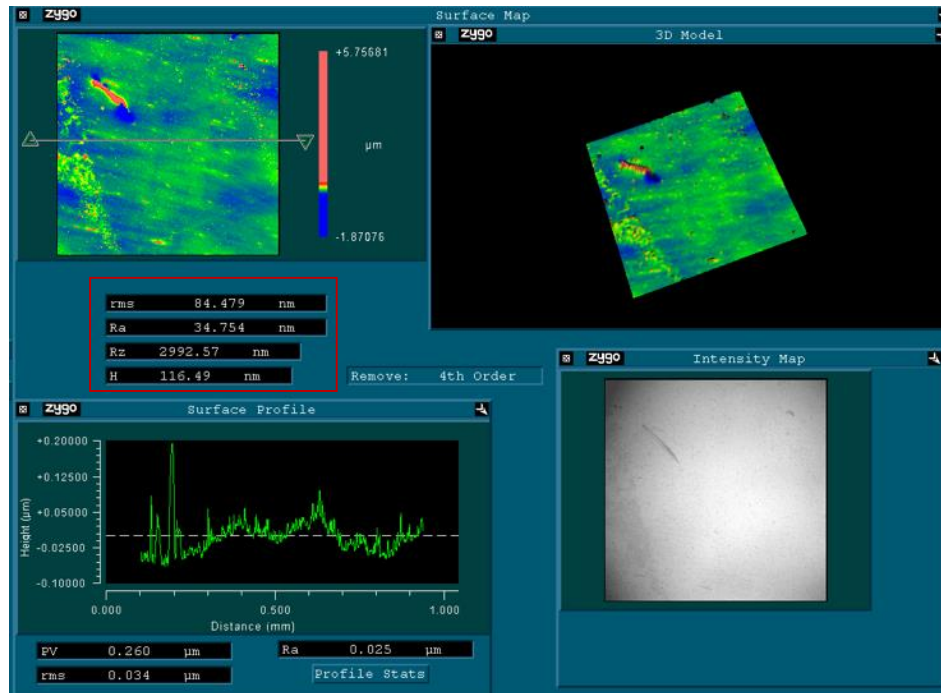


**Figure 15. Calculation of surface roughness parameters (Rq [shown in this software as rms], Ra, Rz, and H) using MetroPro using data collected from a surface of a Penn State PVAD blood sac. Surface roughness parameters are highlighted in red.**

## 2.2 Ovine Study at Penn State Hershey College of Medicine

The Penn State PVAD was tested in juvenile ovine trials at the Penn State Hershey College of Medicine as approved by the Institutional Animal Care and Use Committee. Dorset-Finn lambs were bred for this study. Each sheep had a PVAD surgically implanted after two weeks of monitoring and baseline assessment. The target duration for each trial was 4-6 weeks. Following the completion of the trial, the device was explanted following humane euthanasia of the animal. (20) In each trial, the blood sac was flushed with saline and fixed in formalin for one hour. The blood sacs were examined during the pump teardown for any biological deposits. Documentation of each blood sac was performed by photographing the front, back, top, bottom, inlet side, and outlet side with a digital camera. The location and color of any biological deposits were

documented according to the schematic in Figure 16. Following documentation, the saline was replaced with 1% PFA and the inlet and outlet of the sac were clamped. After fixing for 1 hour, the PFA was rinsed out by pouring 1 L of saline through the inlet. The saline was replaced with PBS and the inlet and outlet were re-clamped. The blood sacs were stored individually in 8 oz. plastic containers in a refrigerator at 4°C until transportation to University Park.

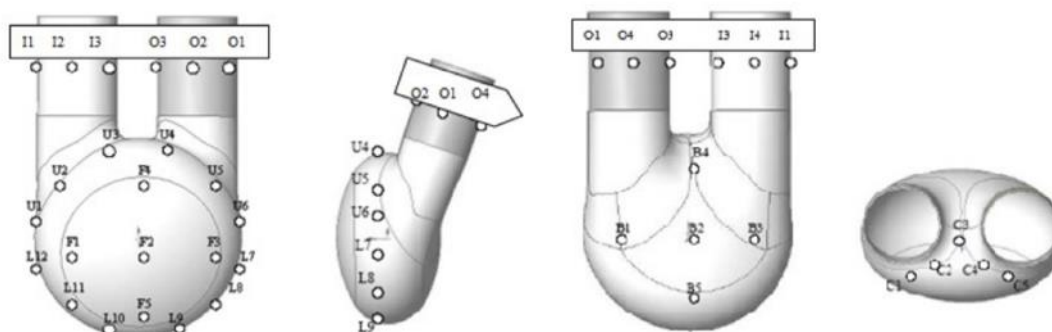


**Figure 16. Schematic of the locations on the blood sac. This diagram is used to describe the locations of deposits and for regions of sampling.**

### 2.3 Sample Preparation and Explanted Sac Analysis

The protocol for the explanted sac analysis was developed and verified by previous members of the Artificial Heart Lab. (33, 34, 35) Following the completion of the ovine trials at the Hershey Medical Center, the SPEUU blood sacs were sent to University Park for analysis. Each blood sac was sampled at twelve regions, as shown in Figure 17. Each sample was cut to the size of 4 mm x 3 mm with a fine scalpel, with the top right corner of the blood-contacting side removed for reference. The samples were prepared with immunofluorescent labeling and imaged with multiple microscopy techniques. Each sample was imaged with a patterned, snaking method as shown in Figure 18 to correlate the images between each technique.

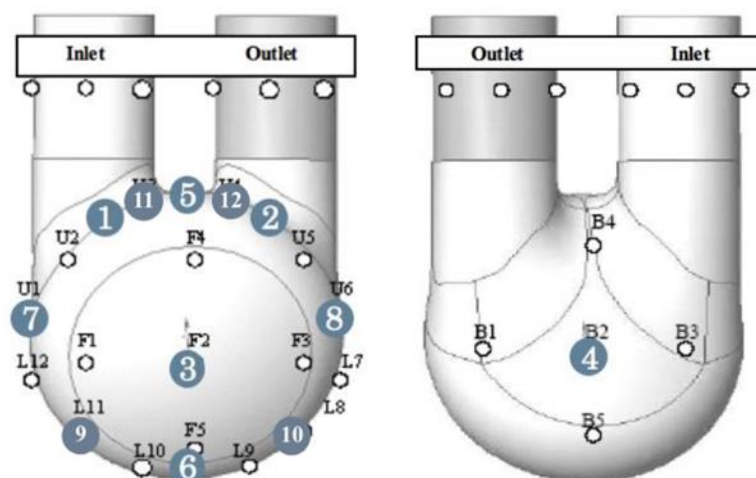


Figure 17. Sampling regions of blood contacting sac. Left: diaphragm side facing forward. Right: stationary side facing forward.

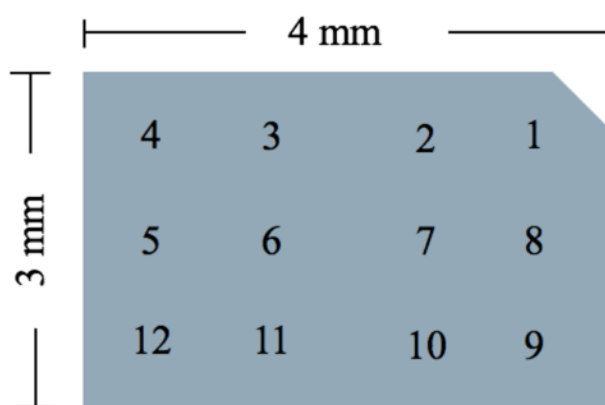


Figure 18. Patterned method for imaging samples. Twelve regions are imaged for each sample. (35)

### 2.3.1 Immunofluorescent Labeling and Confocal Microscopy

Reagents were prepared for the immunofluorescent labeling protocol. The purpose of this protocol is to label platelets and fibrin, so that biological deposits will fluoresce individual colors

when exposed to certain wavelengths of light. The monoclonal anti-fibrinogen (Sigma-Aldrich, St. Louis, Missouri) functions as the primary antibody for fibrin. The CAPP2A IgG1 (Monoclonal Antibody Center, Pullman, Washington) is the primary antibody for platelets. The primary antibodies bind to their respective antigens on the surface of the material. Alexa Fluor® 488 goat anti-mouse IgG (Life Technologies, Grand Island, New York) is a secondary antibody that is used to dye fibrin green. Alexa Fluor® 555 goat anti-mouse IgG (Life Technologies, Grand Island, New York) is used to dye platelets red. The secondary antibodies are tagged with fluorophore and bind to their respective primary antibodies, which generates the fluorescent emission. The permeabilization buffer (PB) was made from bovine serum albumin (Sigma-Aldrich, St. Louis, Missouri) and 1% Triton™ X-100 (Sigma-Aldrich, St. Louis, Missouri) and functions as a blocking agent. The PB is used to prevent nonspecific adsorption of the antibodies to the sample by adsorbing to the sample surface.

Platelets and fibrin were labeled with an indirect method, as shown in Figure 19. This has led to cross-labeling between platelets and fibrin because the host species of both primary antibodies are the same. The method is acceptable because the analysis is meant to identify biological deposits, and differentiation between platelets and fibrin is unnecessary. This method amplifies the fluorescent signal because multiple secondary antibodies can bind to a single primary antibody.

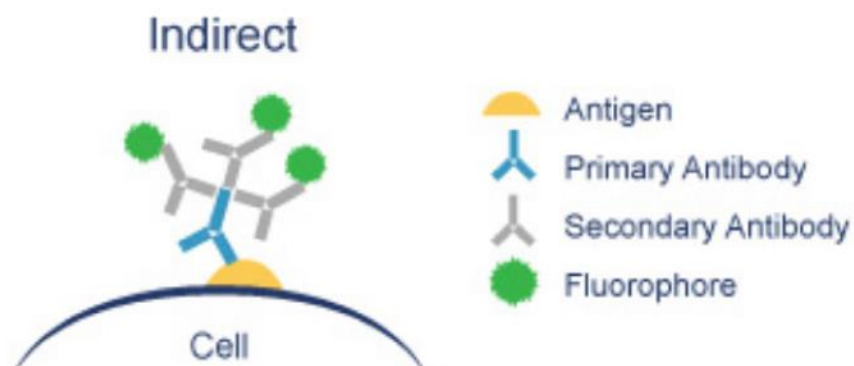


**Figure 19. Indirect immunofluorescent labeling method used for labeling platelets. (42)**

The samples that were cut from each blood sac were placed in the wells of a 12-well tray and were prepared through the following steps:

- Each sample was rinsed with 1 mL of PBS five times.
- The PB was added and the samples incubated for one hour.
- The PB was removed and an anti-fibrinogen/PB solution was added for one hour.
- The anti-fibrinogen/PB solution was removed and the samples were rinsed with PBS three times.
- Alexa Fluor 488 was added and the samples incubated in the dark for one hour. From this point until confocal microscopy, the samples were kept in the dark.
- The Alexa Fluor 488 was removed and the samples were rinsed three times with PBS.
- The PB was added for one hour.
- The PB was removed and CAPP2A was added for one hour.

- The CAPP2A was removed and the samples were rinsed three times with PBS.
- Alexa Fluor 555 was added for one hour.
- Alexa Fluor 555 was removed and the samples were rinsed three more times with PBS.

All reagents used during the labeling process were added in 1 mL quantities and all incubation took place at room temperature.

The 488 nm and 543 nm lasers on the Olympus Fluoview 1000 confocal microscope (Olympus America Inc., Center Valley, Pennsylvania) at the Huck Institute of Life Sciences were used to image the fluorescent platelets and fibrin. A 20x dry objective was used for the 12 snaking images. The 60x oil objective or the 100x dry objective were used on specific areas of interest.

### **2.3.2 Environmental Scanning Electron Microscopy**

After the imaging on the confocal microscope was completed, the samples were rinsed 5 times with deionized (DI) water and prepared for imaging with the ESEM to confirm the fluorescence seen on confocal. The samples were mounted onto SEM stubs with carbon tape and placed in the Quanta 200 or 250 Environmental SEM (FEI, Hillsboro, Oregon) in the Materials Characterization Lab of the Materials Research Institute. Low vacuum mode, at a pressure of 60 Pa, was used to dissipate the charge of the uncoated samples. High voltage mode with an accelerating voltage of 15 kV was also used. Each region was imaged at a 150x magnification for each of the 12 regions per sample. Areas of interest were examined at higher magnifications as needed.

### **2.3.3 Degradation of Biological Deposits**

After ESEM imaging, all biologics were degraded from the polymer surface to obtain better view of the true surface of the SPEUU material. Pepsin (Sigma-Aldrich, St. Louis, Missouri) and hydrochloric acid were combined in a 3:1 ratio and 2 mL of this solution was added to each sample. The samples incubated for 3 hours at 37°C. Following incubation, the samples were rinsed 5 times with DI water and placed on glass slides with double-sided tape in preparation for imaging on the optical profilometer. If any biological deposits did not appear to fully degrade from the surface, the degradation protocol was repeated.

### **2.3.4 Optical Profilometry**

The Zygo NexView 7300 optical profilometer (Zygo Corporation, Middlefield, Connecticut) in the Materials Characterization Lab of the Materials Research Institute was used to evaluate the surface of the sac samples. The 12 images for each sample were taken using a 20x lens with a 0.5x zoom lens. The coherence scanning interferometry (CSI) measure mode, with a z resolution set to high, was used and the scan length was adjusted as needed to include all data points. The data were then analyzed on MetroPro® 8.3.5 software where surface roughness parameters were copied onto an Excel sheet for further analysis. A 4th-order remove function was applied to eliminate differences in samples caused by the curvature of the sac. Each sample was examined to determine if debris, remaining biologics, or curvature on the edge of a sample were present from the profilometry images. These elements would lead to inaccurate surface roughness parameters because they block the true surface of the material. Figure 20 shows an example of a the MetroPro interface on a sample where there is a piece of debris on the surface. Figure 21 shows

the surface topography without and with masking. The roughness parameters decrease in value after masking is applied, demonstrating that the presence of debris, remaining biologics, or curvature from the edge of the sample have an impact on the roughness analysis of the blood sacs and need to be removed.

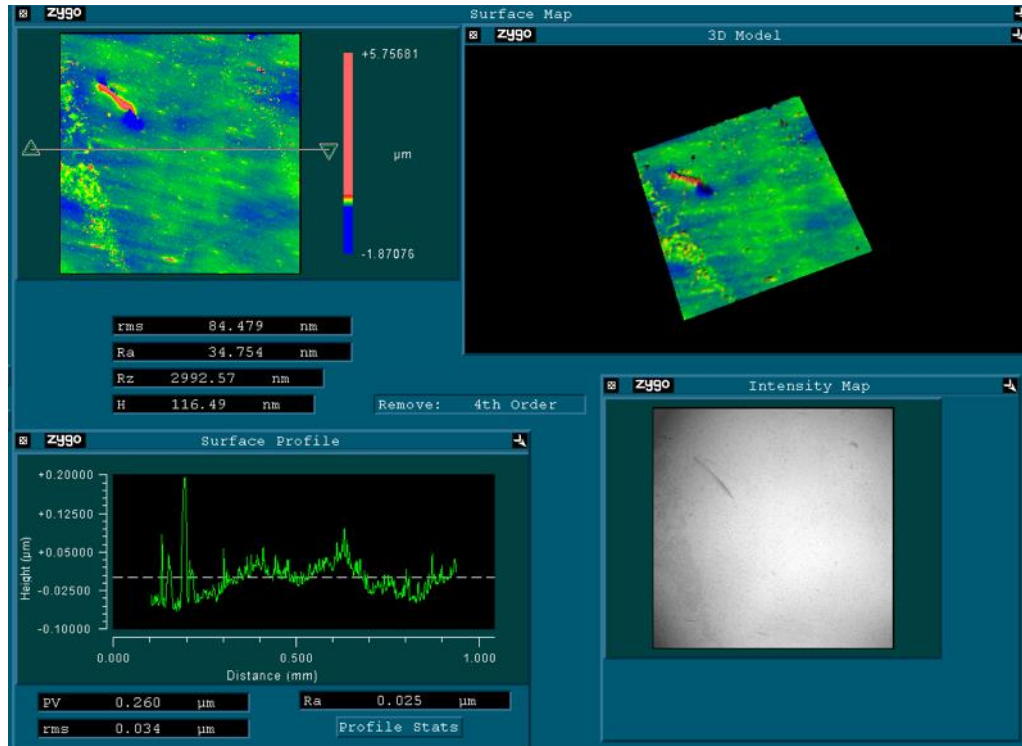


**Figure 20.** The MetroPro interface shows a piece of debris with elevated topography on the 3D model. This is an example of an area that would be masked and removed from surface analysis.

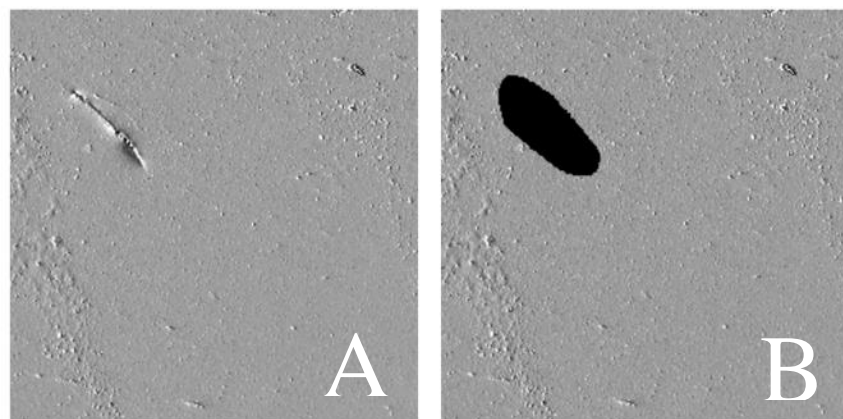


**Figure 21. An example of a profilometry image from Sac 249, Sample 4, Region 3 (A) without masking and (B) with masking applied.**

## **Chapter 3**

### **Results**

#### **3.1 Explanted Sac Analysis**

There were 13 blood sacs evaluated at 12 sampling locations, as shown in Figure 17. This study adds to previous work with the analysis of Sacs 151 and 240 at all 12 sampling locations and evaluates all blood sacs at the additional sampling locations 9-12. The results described are comprehensive of all data gathered on this project.

The confocal and ESEM images were used to identify the presence and location of thrombosis on the blood sacs following the ovine trials. The locations and sizes of deposition were noted. To understand the relationship between thrombosis and surface roughness, images from confocal and ESEM were compared with data from optical profilometry. This correlation was possible because of the patterned imaging technique described in Section 2.3. Images taken for the same location by different techniques were compared for each sample. Section 3.1.1 provides 12 tables that summarize the size of the deposits at each location. The deposits have irregular shapes, so the diameters are estimates to show relative sizes. Macroscopic deposits were defined as being seen with the naked eye prior to imaging and have approximate diameters larger than 150  $\mu\text{m}$ . Microscopic deposits were defined as not being visible with the naked eye but were visible with confocal and ESEM. These deposits have approximate diameters smaller than 150  $\mu\text{m}$ .

### 3.1.1 Deposit Sizes by Location

**Table 1. Deposits at Location 1: Inlet**

Sac Number	Deposit Location	Approximate Diameter of Deposit ( $\mu\text{m}$ )
170	Regions 8-9	400
176	Region 2	10
183	Regions 6-11	2000 (patch)

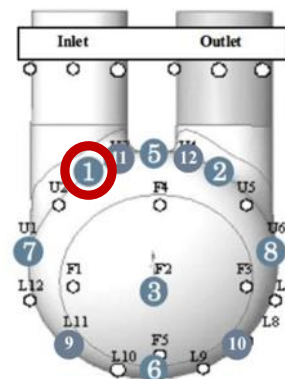


**Table 2. Deposits at Location 2: Outlet**

Sac Number	Deposit Location	Approximate Diameter of Deposit ( $\mu\text{m}$ )
170	Regions 5 and 7	40, 15
183	Regions 1-8	3000 (patch)
190	Regions 6-7 and 10-11	800
232	Region 6	10
234	Regions 5-12	3000 (patch)
240	Region 7	20

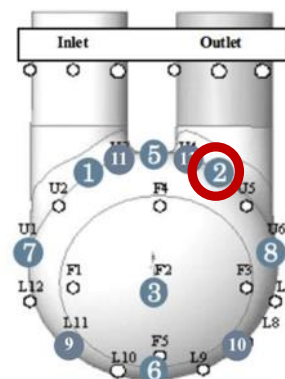


**Table 3. Deposits at Location 3: Center Front**

Sac Number	Deposit Location	Approximate Diameter of Deposit ( $\mu\text{m}$ )
170	Regions 7 and 8	15, 20
183	Region 4	10
192	Region 9	15
234	Region 5	60
247	Region 2	15

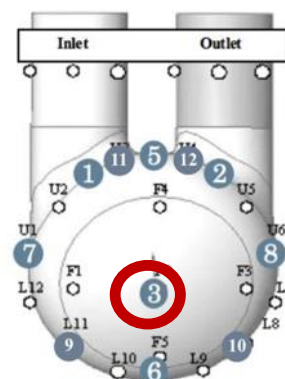


**Table 4. Deposits at Location 4: Center Back**

Sac Number	Deposit Location	Approximate Diameter of Deposit ( $\mu\text{m}$ )
190	Region 6	100
192	Region 11	80
223	Region 4	10
247	Region 12	10, 10

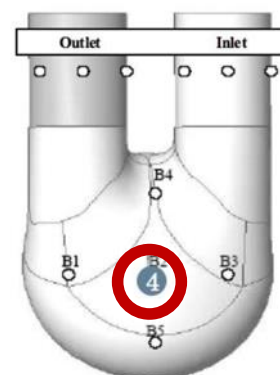


**Table 5. Deposits at Location 5: Top**

Sac Number	Deposit Location	Approximate Diameter of Deposit ( $\mu\text{m}$ )
172	Region 4	50
183	Region 2	30
223	Regions 3 and 11	80, 30
249	Region 3	40

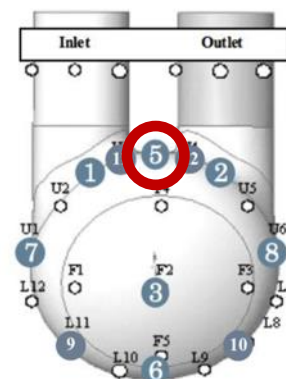


**Table 6. Deposits at Location 6: Bottom**

Sac Number	Deposit Location	Approximate Diameter of Deposit ( $\mu\text{m}$ )
240	Regions 4 and 11	40, 15
249	Region 2	10

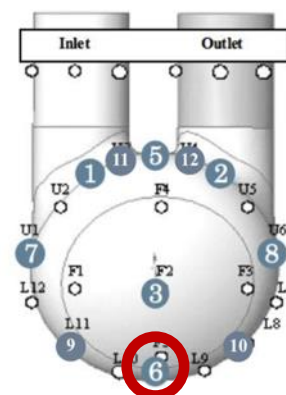


Table 7. Deposits at Location 7: Inlet Side

Sac Number	Deposit Location	Approximate Diameter of Deposit ( $\mu\text{m}$ )
172	Region 5	50
223	Region 11	40
247	Region 10	20

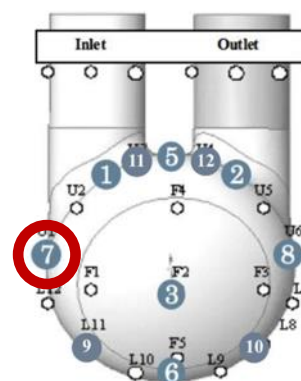


Table 8. Deposits at Location 8: Outlet Side

Sac Number	Deposit Location	Approximate Diameter of Deposit ( $\mu\text{m}$ )
183	Regions 5-6	800 (scattered)
249	Region 2	10

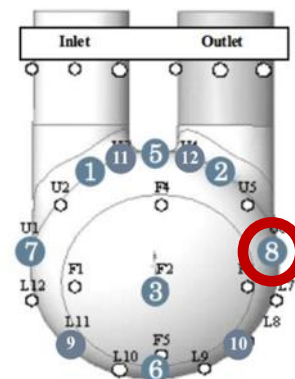
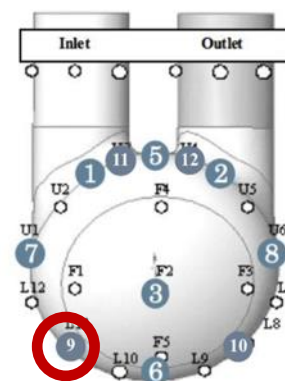


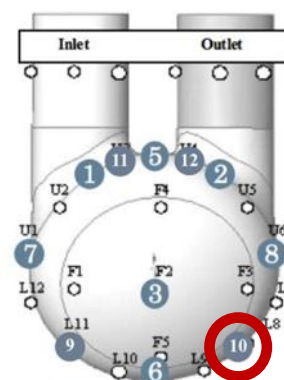
Table 9. Deposits at Location 9: Inlet Bottom

Sac Number	Deposit Location	Approximate Diameter of Deposit ( $\mu\text{m}$ )
223	Region 5	150

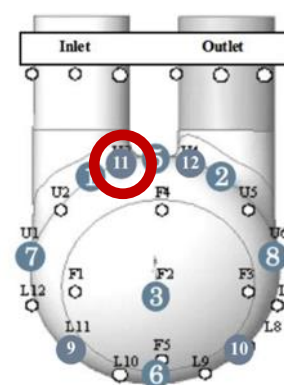


**Table 10. Deposits at Location 10: Outlet Bottom**

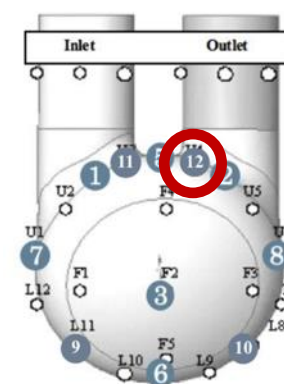
Sac Number	Deposit Location	Approximate Diameter of Deposit ( $\mu\text{m}$ )
234	Region 4	10

**Table 11. Deposits at Location 11: Inlet Top**

Sac Number	Deposit Location	Approximate Diameter of Deposit ( $\mu\text{m}$ )
170	Region 12	10
172	Region 7	20
190	Region 12	250 (scattered)
240	Region 9	10

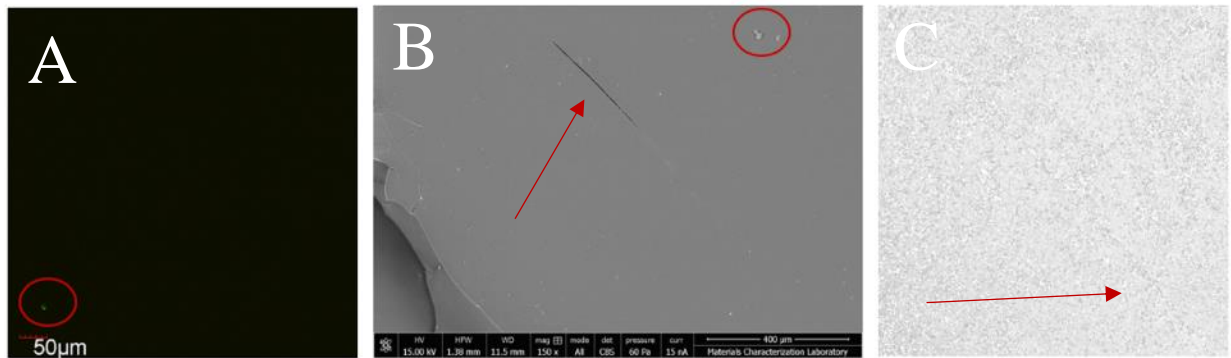
**Table 12. Deposits at Location 12: Outlet Top**

Sac Number	Deposit Location	Approximate Diameter of Deposit ( $\mu\text{m}$ )
183	Regions 1-8	3000 (patch)
190	Regions 11-12	800 (scattered)
223	Region 8	5
240	Region 12	30



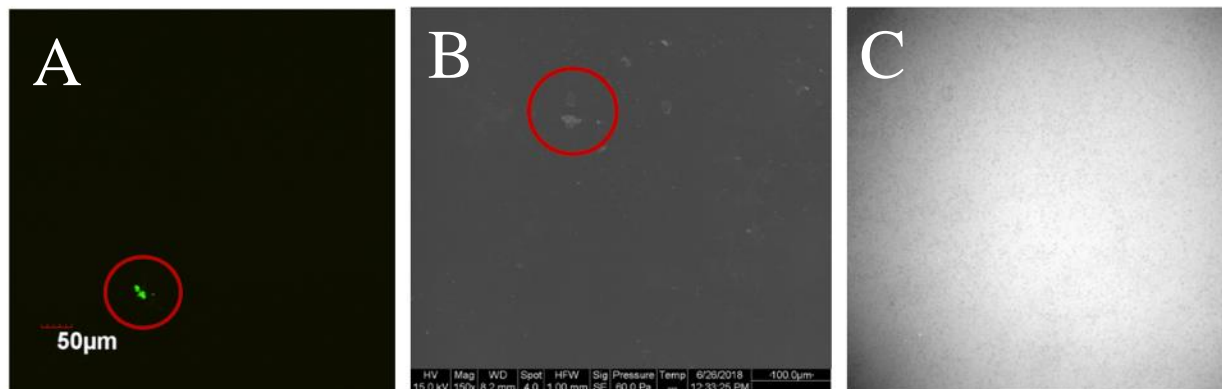
### 3.1.2 Correlation of Confocal, ESEM, and Profilometry

To study the relationship between surface roughness and thrombosis, the confocal, ESEM, and profilometry images were correlated. For the smaller deposits, it was more difficult to correlate the confocal and ESEM images. However, inferences were drawn from the size and structure of the deposits. Figure 22 shows images from region 12 on the inlet top sample of Sac 170. A small, green deposit with a diameter of approximately 10  $\mu\text{m}$  was located. The profilometry images show a smooth surface with one scratch correlated between the ESEM and profilometry images.



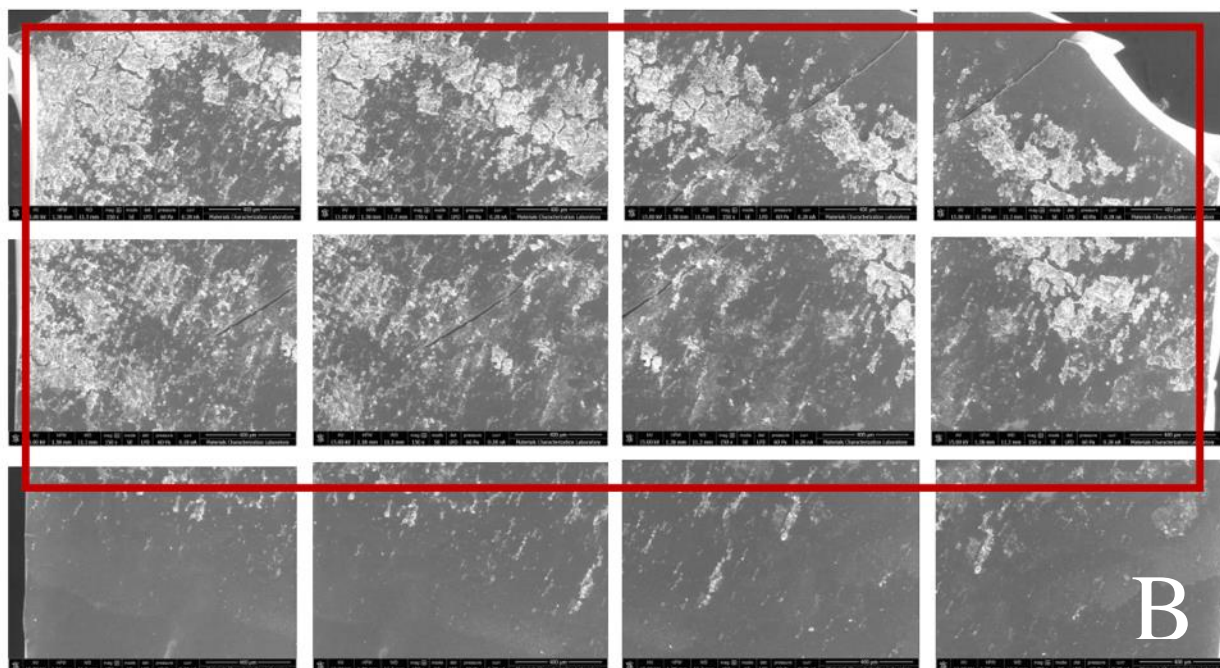
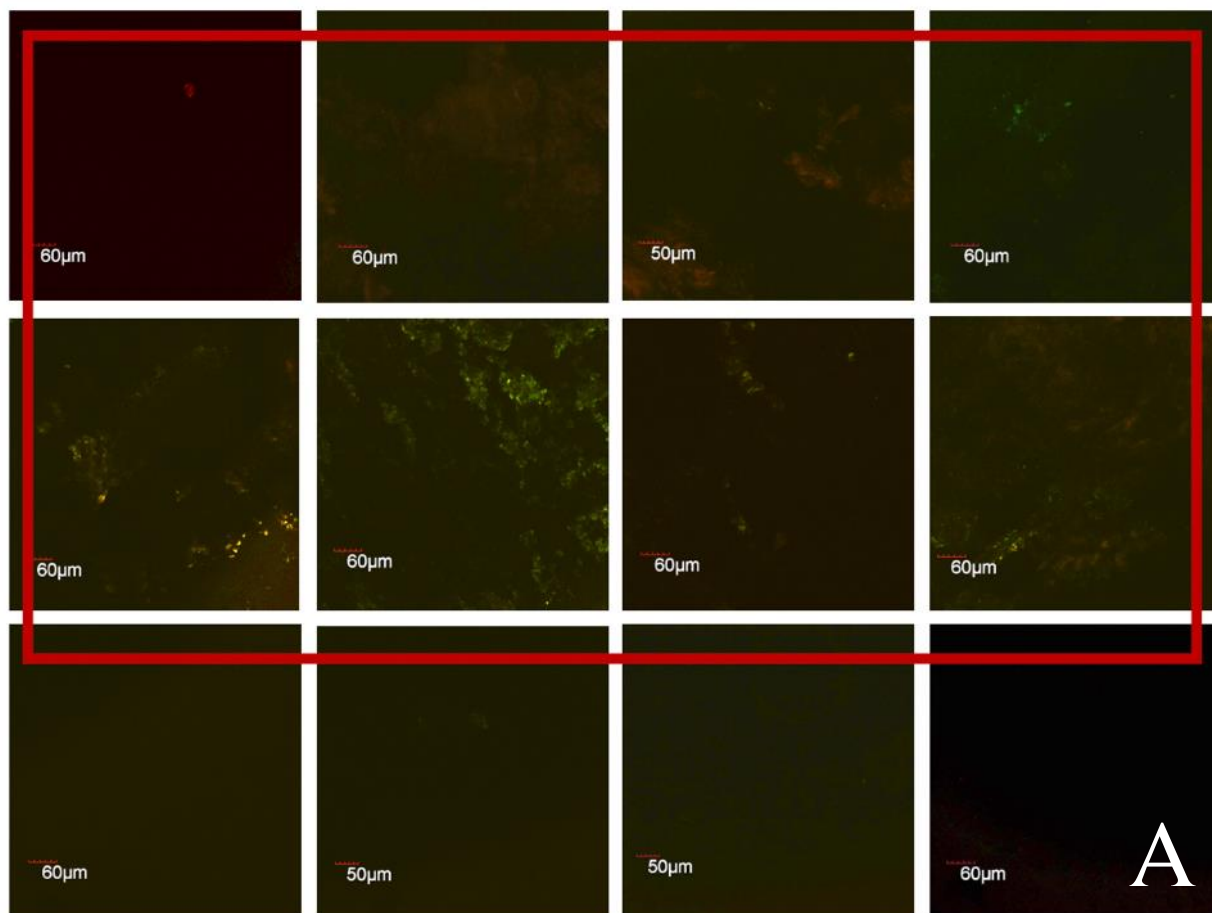
**Figure 22. Correlation of (A) confocal, (B) ESEM, and (C) profilometry images on the inlet of Sac 170. There is a small microscopic deposit circled in red and a scratch shown by the arrows.**

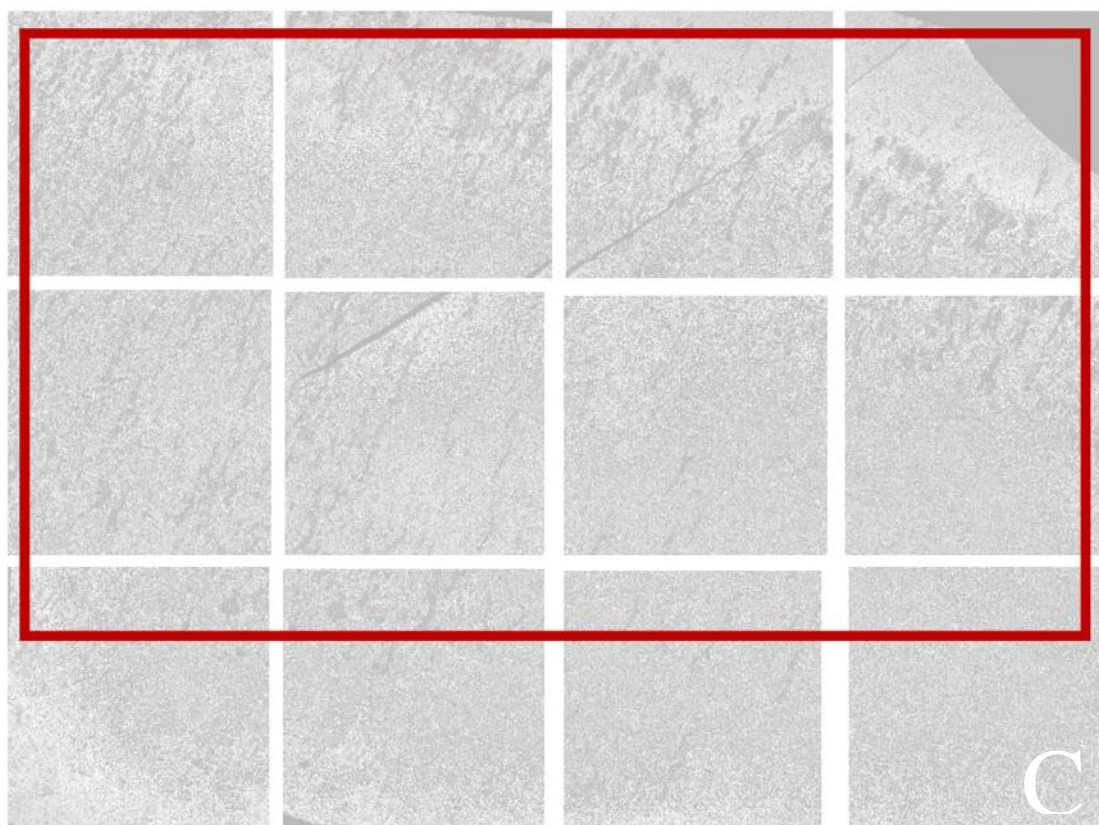
From Sac 172, there was a slightly larger green deposit found on region 7 of the inlet top sample, shown in Figure 23. This deposit was approximately 20  $\mu\text{m}$  in diameter. The profilometry image shows that the surface is relatively smooth.



**Figure 23. Correlation of (A) confocal, (B) ESEM, and (C) profilometry images on the inlet top of Sac 172. There is a small microscopic deposit circled in red.**

Sac 183 featured the most significant deposition that spanned across the entire sample at the outlet top, as presented in parts A, B, and C of Figure 24. The deposit covered a patch of approximately 4000 x 2000  $\mu\text{m}$ . The biologics were degraded twice but did not fully degrade. Remaining biologics were masked out of the data collection so that only the true surface of the material was analyzed for roughness.

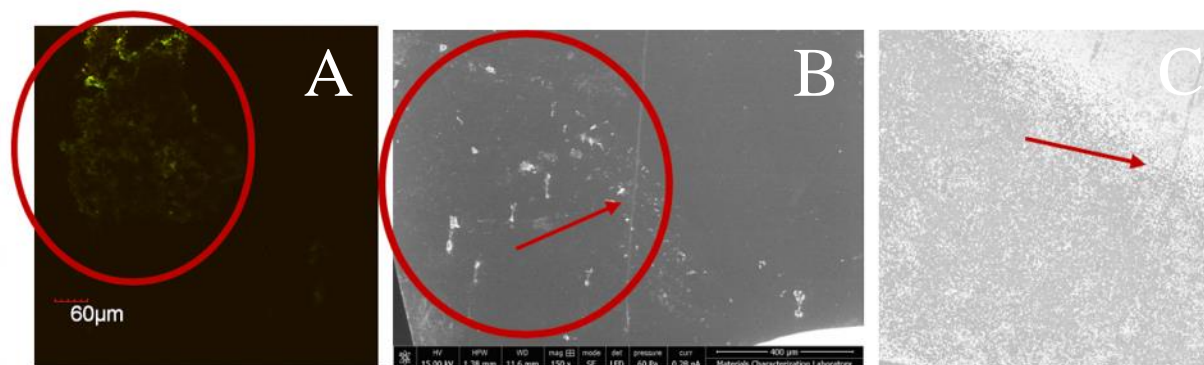




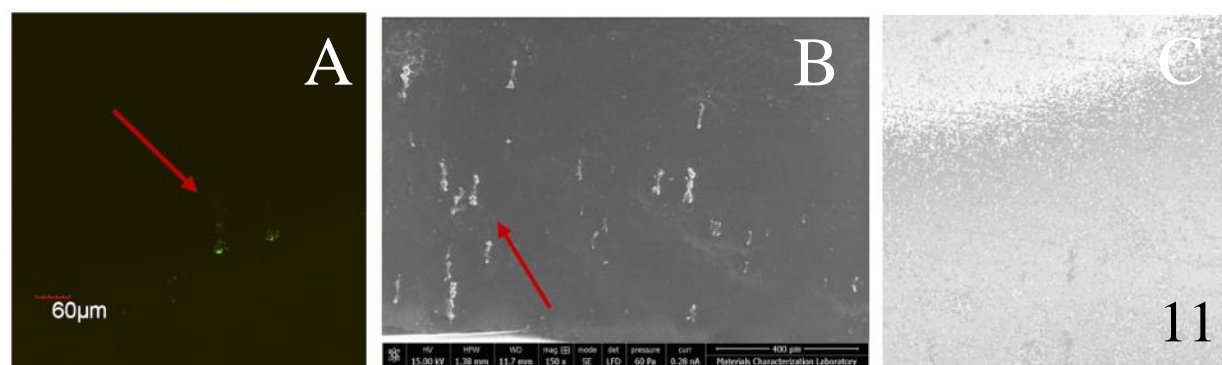
**Figure 24. Correlation of (A) confocal, (B) ESEM, and (C) profilometry images on the outlet top of Sac 183. There is large macroscopic deposition shown within the red boxes. Topography shows some residual biologics.**

Sac 190 showed deposition on the inlet top (Figure 25) and the outlet top (Figure 26). The inlet top showed some scattered deposition across region 12 of the sample. The confocal image shows a large deposit with a diameter of approximately 250  $\mu\text{m}$  and the ESEM image shows biologics in the same region. The biologics on the ESEM image are small and scattered across the surface. The topography shows a scratch on the surface. The outlet top showed a similar pattern of deposition, but it spanned across two regions of the sample. The biologics range from about 20

$\mu\text{m}$  in diameter to about  $80\ \mu\text{m}$  in diameter. These deposits cover a patch of approximately  $2000 \times 800\ \mu\text{m}$ . The traces of residual biologics were masked from the data collection.



**Figure 25. Correlation of (A) confocal, (B) ESEM, and (C) profilometry of the inlet top of Sac 190. There is scatted deposition circled in red. The arrows point to a scratch on the surface.**



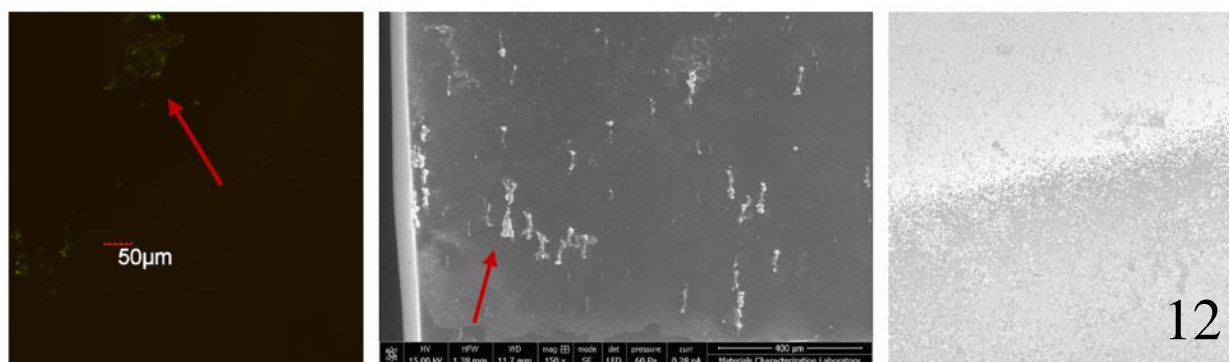


**Figure 26. Correlation of (A) confocal, (B) ESEM, and (C) profilometry of the outlet top of Sac 190. Scattered deposition is shown by the red arrows and spreads across regions 11 and 12.**

Sac 223 showed deposits at the inlet bottom (Figure 27) and the outlet top (Figure 29). The macroscopic deposit on the inlet bottom had a diameter of approximately 150  $\mu\text{m}$ . The structure is clearly verified by ESEM. Significant biologics remained on the topography, even after the sample was degraded three times. The surface map of this deposit is shown in Figure 28. The 3D model shows that the topography is raised above the surface. The biologics were masked from the data collection. There was a very small, microscopic deposit found on the outlet top.



**Figure 27. Correlation of (A) confocal, (B) ESEM, and (C) profilometry on the inlet bottom of Sac 223. There is a large macroscopic deposit seen on the surface. The biologics were not fully degraded from the profilometry image.**

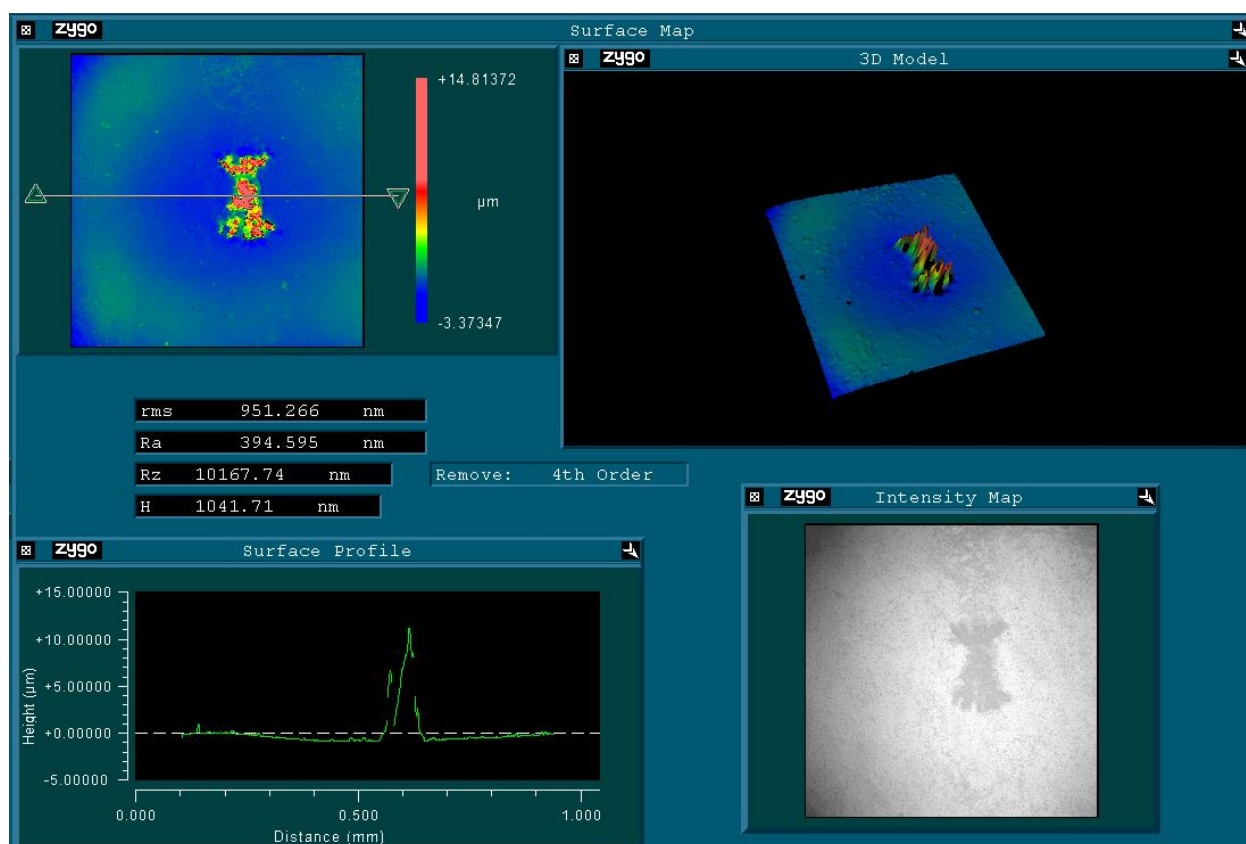


**Figure 28.** MetroPro analysis for region 5 of the inlet bottom on Sac 223. The 3D model and surface profile show the raised topography in the area of interest.



**Figure 29.** Correlation of (A) confocal, (B) ESEM, and (C) profilometry on the outlet top of Sac 223. There is a small, macroscopic deposit shown in the red circles.

Sac 234 showed a small, microscopic deposit on the outlet bottom, as shown in Figure 30. This deposit had an approximate diameter of 10  $\mu\text{m}$ . The topography appeared smooth on the profilometry image.

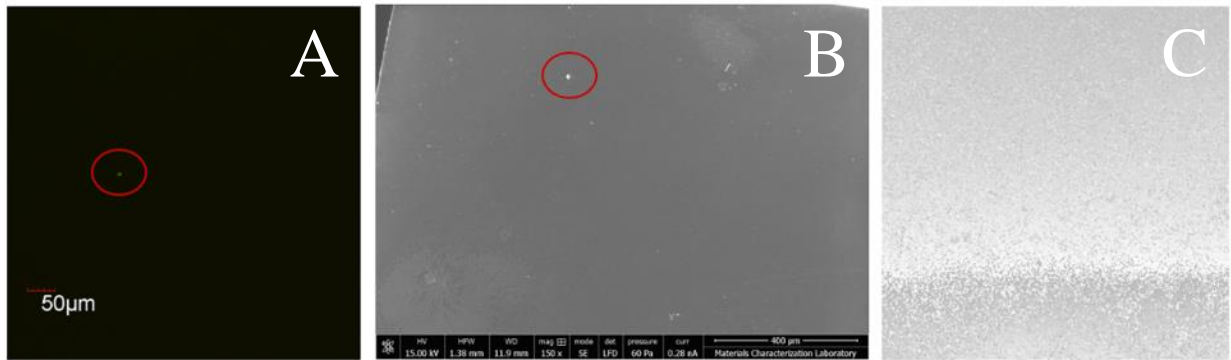


**Figure 30. Correlation of (A) confocal, (B) ESEM, and (C) profilometry on the outlet bottom of Sac 234. There was a small, microscopic deposit shown by the red circles.**

Sac 240 showed microscopic deposits near the outlet (Figure 31), bottom (Figure 32), inlet top (Figure 33), and outlet top (Figure 34). The deposit at the outlet was about 20  $\mu\text{m}$  in diameter. The bottom of Sac 240 showed deposits in region 4 and region 11, with sizes of approximately 30  $\mu\text{m}$  and 15  $\mu\text{m}$ , respectively. The inlet top showed a small deposit with a 10  $\mu\text{m}$  diameter and the outlet top showed a deposit with a 30  $\mu\text{m}$  diameter. The outlet top showed a scratch, visible on the ESEM and profilometry images. The sample was examined by ESEM with the blood contacting side facing up and with the non-blood contacting side facing up to understand whether the scratch was on the inside or the outside of the blood sac. The scratch was only visible from the blood contacting side, verifying that the scratch was on the inside of the blood sac.



Figure 31. Correlation of (A) confocal, (B) ESEM, and (C) profilometry on the outlet of Sac 240. There is a microscopic deposit shown by the red circles.

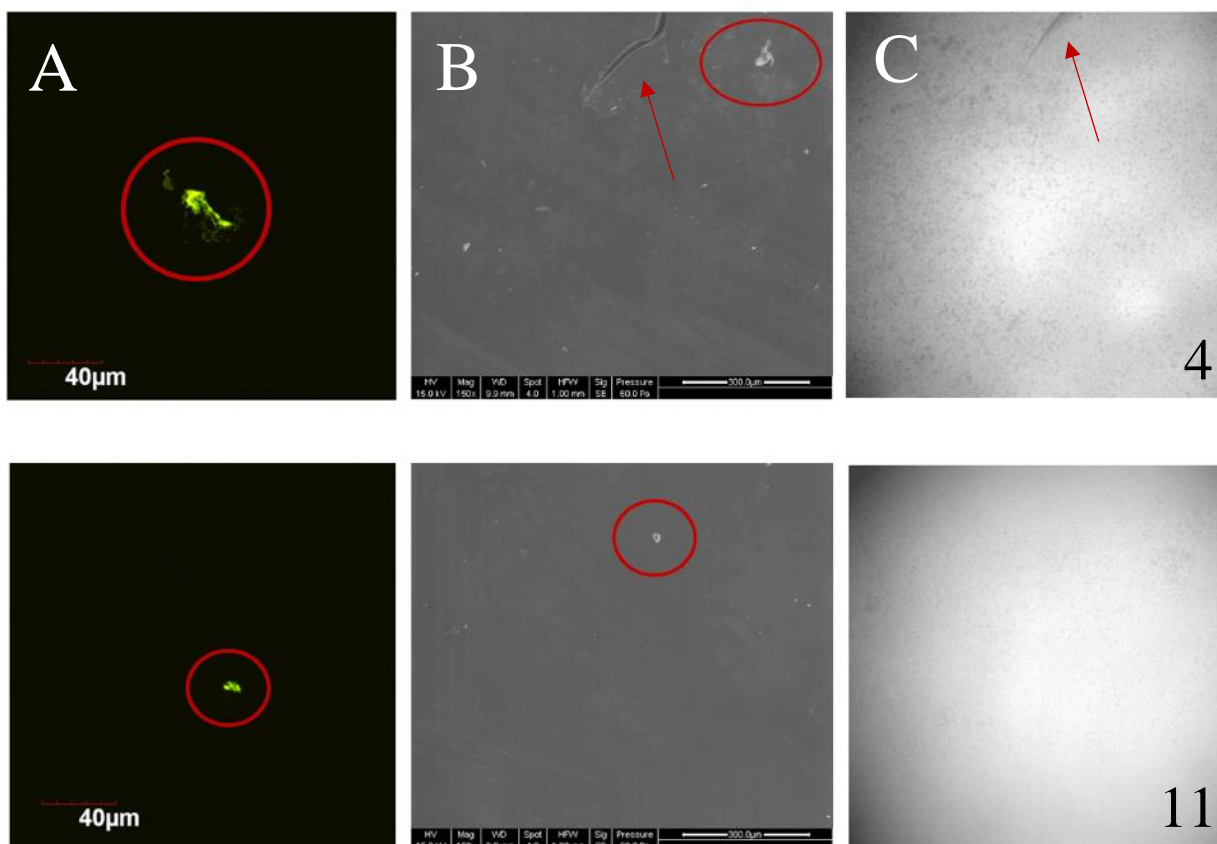


Figure 32. Correlation of (A) confocal, (B) ESEM, and (C) profilometry on the bottom of Sa 240. There is a moderate microscopic deposit on region 4 and a small microscopic

deposit on region 11 shown by the red circles. There is a scratch on region 4 that is shown by the red arrows.

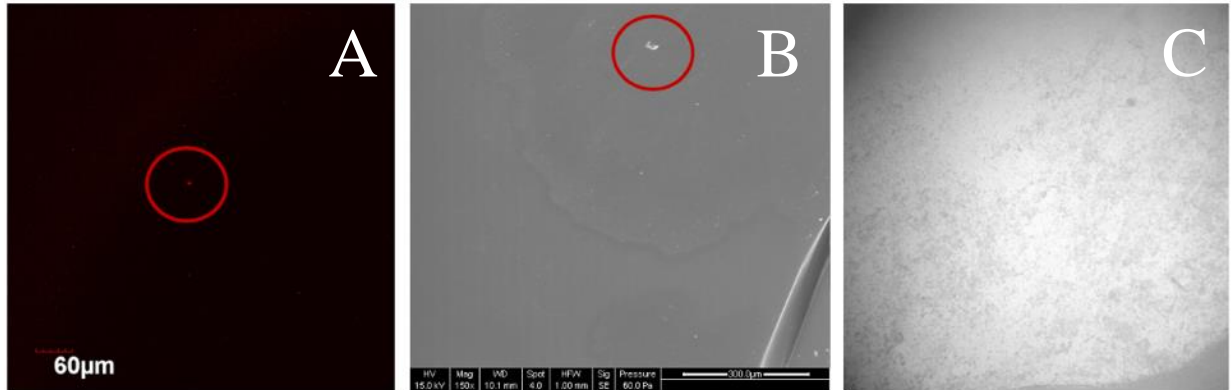


Figure 33. Correlation of (A) confocal, (B) ESEM, and (C) profilometry on the inlet top of Sac 240. There is a small microscopic deposit shown by the red circles.

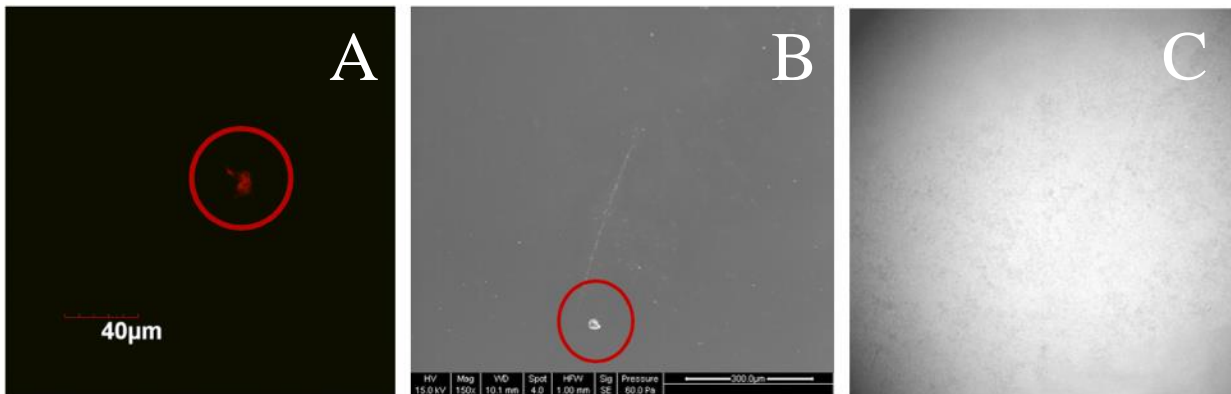
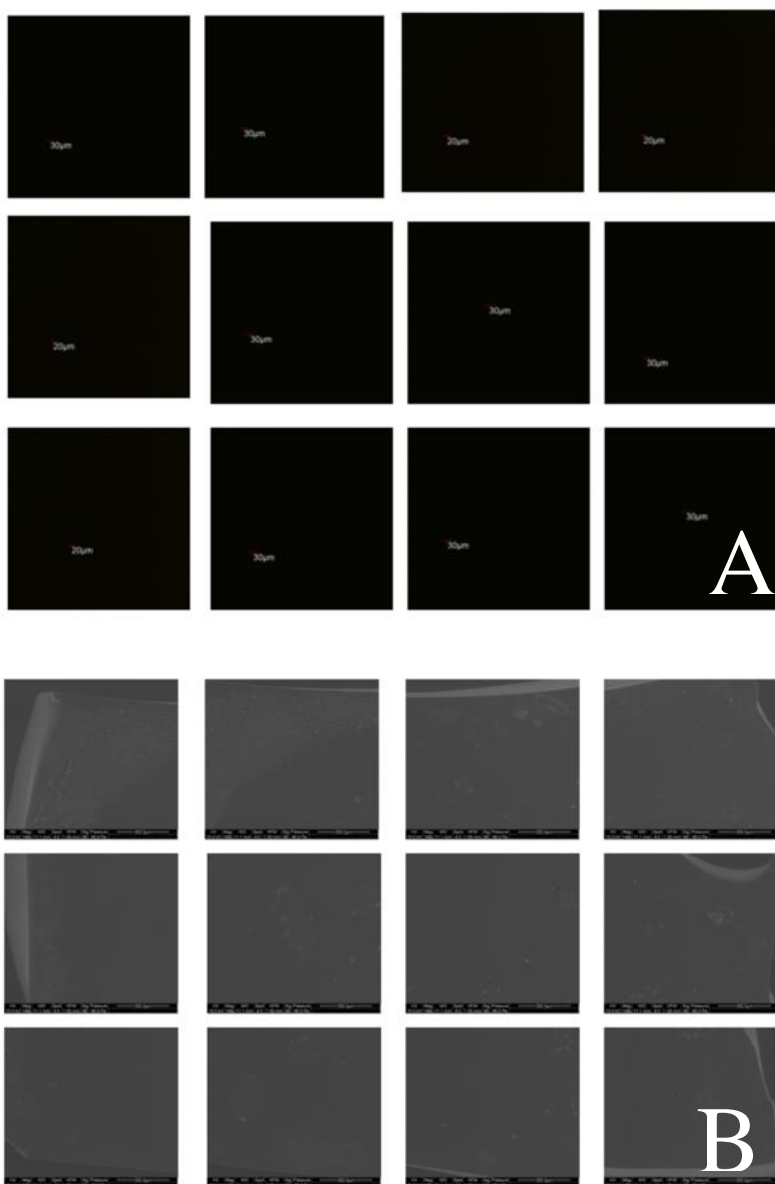


Figure 34. Correlation of (A) confocal, (B) ESEM, and (C) profilometry on the outlet top of Sac 240. There is a microscopic deposit shown by the red circles.

### 3.2 Controls

In the previous study, a control sac was tested with the explanted sac protocol. This blood sac was never in contact with blood. Figure 35 shows the images taken of the control sac from confocal (Figure 35-A) and ESEM (Figure 35-B). As expected, the control sac showed no

fluorescence due to the lack of contact with blood. The profilometry data from the control sac were used in comparison with the samples that showed evidence of deposition.



**Figure 35. Images taken by confocal (A) and ESEM (B) of the control sac. No fluorescence is noted.**

### 3.3 Surface Roughness Analysis

The data were organized by macroscopic size and microscopic size, as shown in Tables 13 and 14. Surface roughness parameters were gathered for each sample. The sample locations marked with \* underwent the pepsin degradation at least one additional time. The approximate sizes that are denoted by “patch” means that the sample is nearly covered with deposition across the entire area. The sizes that are denoted by “scattered” describes that multiple microscopic deposits are clustered and scattered across the area given, but the entire area is not covered by deposition. The sizes that are separated by a comma demonstrates that there were multiple biological deposits on that sample.

**Table 13. Summary of Roughness Data for Macroscopic Deposits**

<b>Sac Number</b>	<b>Sample Location</b>	<b>Approximate Diameter of Deposit (μm)</b>	<b>Rq (nm)</b>	<b>Ra (nm)</b>	<b>Rz (nm)</b>	<b>H (nm)</b>
170	inlet*	400	156.49	95.97	5375.1	351.34
183	inlet*	2000 (patch)	146.3	79.37	3495.7	278.2
	outlet*	3000 (patch)	243.43	115.71	5180.1	429.8
	outlet top*	3000 (patch)	260.24	151.66	5064.5	609.7
190	outlet*	800	177.72	115.6	3041.6	450.9
223	inlet bottom*	150	148.91	91.226	4992.1	313.8
234	outlet*	3000 (patch)	130.56	85.2	2638.3	309.9

**Table 14. Summary of Roughness Data for Microscopic Deposits**

<b>Sac Number</b>	<b>Sample Location</b>	<b>Approximate Diameter of Deposit (μm)</b>	<b>Rq (nm)</b>	<b>Ra (nm)</b>	<b>Rz (nm)</b>	<b>H (nm)</b>
170	outlet	40, 15	163.5	104.2	6785.8	404.2
	center front	15, 20	98.3	56.7	2422.6	239.4
	inlet top	10	94.2	63.2	3218.9	227.2
172	top	50	187.1	125.3	3343.5	444.6
	inlet side	50	164.7	84.3	8095.3	296.1
	inlet top	20	136.5	105.0	1707.0	384.5
176	inlet	10	186.5	110.5	11243.0	412.9
183	center front	10	71.8	31.7	3605.5	111.4
	top	30	133.0	86.6	3820.9	313.3
	outlet side	800 (scattered)	108.1	62.2	3649.7	207.5
190	center back	100	120.7	61.4	5505.1	206.1
	inlet top	250 (scattered)	122.5	82.5	3715.8	304.1
	outlet top	800 (scattered)	111.2	69.5	3694.1	250.1
192	center front	15	121.1	60.4	4268.7	226.8
	center back	80	110.4	66.0	3166.4	225.3
223	center back	10	131.2	80.3	2597.1	334.9
	top	80, 30	173.9	121.7	3810.1	444.7
	inlet side	40	158.2	81.1	5109.7	320.7
	outlet top	5	83.4	57.6	1891.0	214.2
232	outlet	10	184.3	103.8	5397.1	384.0
234	center front	60	76.0	35.7	23708.0	123.4
	outlet bottom	10	156.0	112.2	2872.3	407.0
240	outlet	20	116.0	69.3	7389.4	267.7
	bottom	30, 15	151.2	91.7	10063.0	352.3
	inlet top	10	176.3	104.7	11555.0	388.7
	outlet top	30	146.9	92.4	10100.0	346.2
247	center front	15	112.8	52.8	3666.1	179.8
	center back	10, 10	84.5	43.9	2580.2	157.9
	inlet side	20	79.4	50.9	2090.3	179.2
249	top	40	159.6	87.7	5411.2	297.5
	bottom	10	96.7	54.0	3529.2	191.2
	outlet side	10	125.9	53.0	4998.0	180.5

After the 13 sac analyses were completed, the locations of the deposits were noted. Figure 36 provides a map of all deposits found over the 13 sacs. There were 7 macroscopic deposits and 32 microscopic deposits. Most of the deposits were located along the upper ridge near the inlet, top, or outlet.

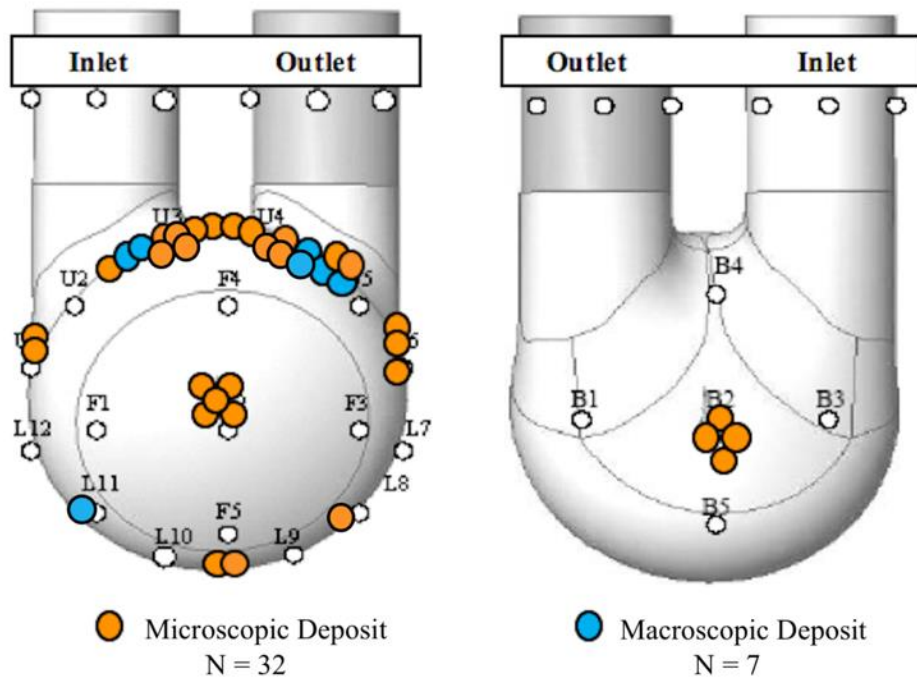


**Figure 36. Map of all deposits for the 13 sacs analyzed.**

The samples containing macroscopic and microscopic deposits were analyzed to determine if the topography under the deposition was rougher than the control topography. Figure 37 shows a comparison of the roughness parameters  $R_q$ ,  $R_a$ , and  $H$  for macroscopic, microscopic, and control samples. For  $R_q$ , the macroscopic regions showed values 62% higher than the control and 28% higher than the microscopic regions. The microscopic regions were 47% higher than the control. For  $R_a$ , the macroscopic regions showed values 61% higher than the control and 26% higher than the microscopic regions. The microscopic regions were 47% higher than the control.

For H, the macroscopic regions were 63% higher than the control and 28% higher than the microscopic regions. The microscopic regions were 49% higher than the control.

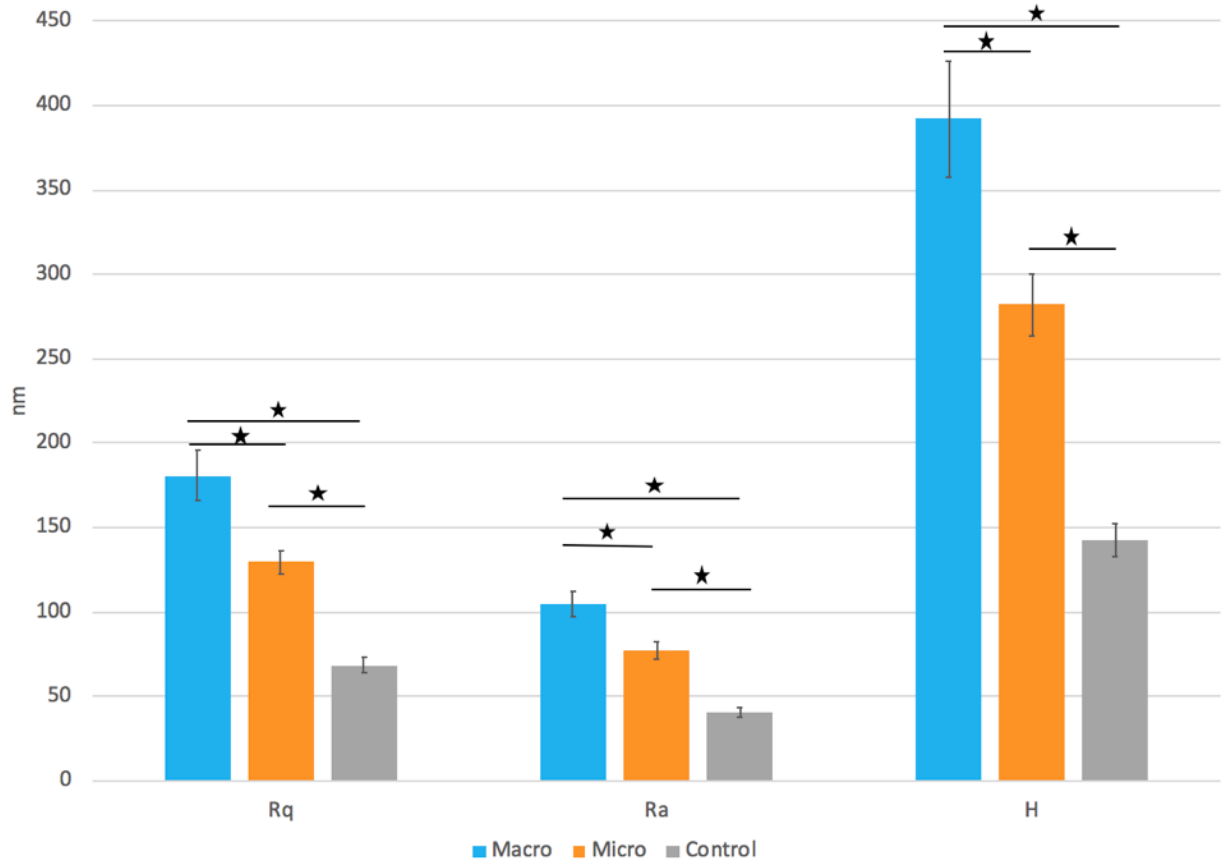


**Figure 37. Comparing average Rq, Ra, and H values between macroscopic and microscopic deposits and a control sac. Error bars indicate the standard error of the mean.**

Figure 38 shows a comparison of Rz for the macroscopic, microscopic, and control samples. For Rz, the macroscopic regions showed values 28% lower than the microscopic regions and 53% higher than the control. The microscopic regions were 63% higher than the control.

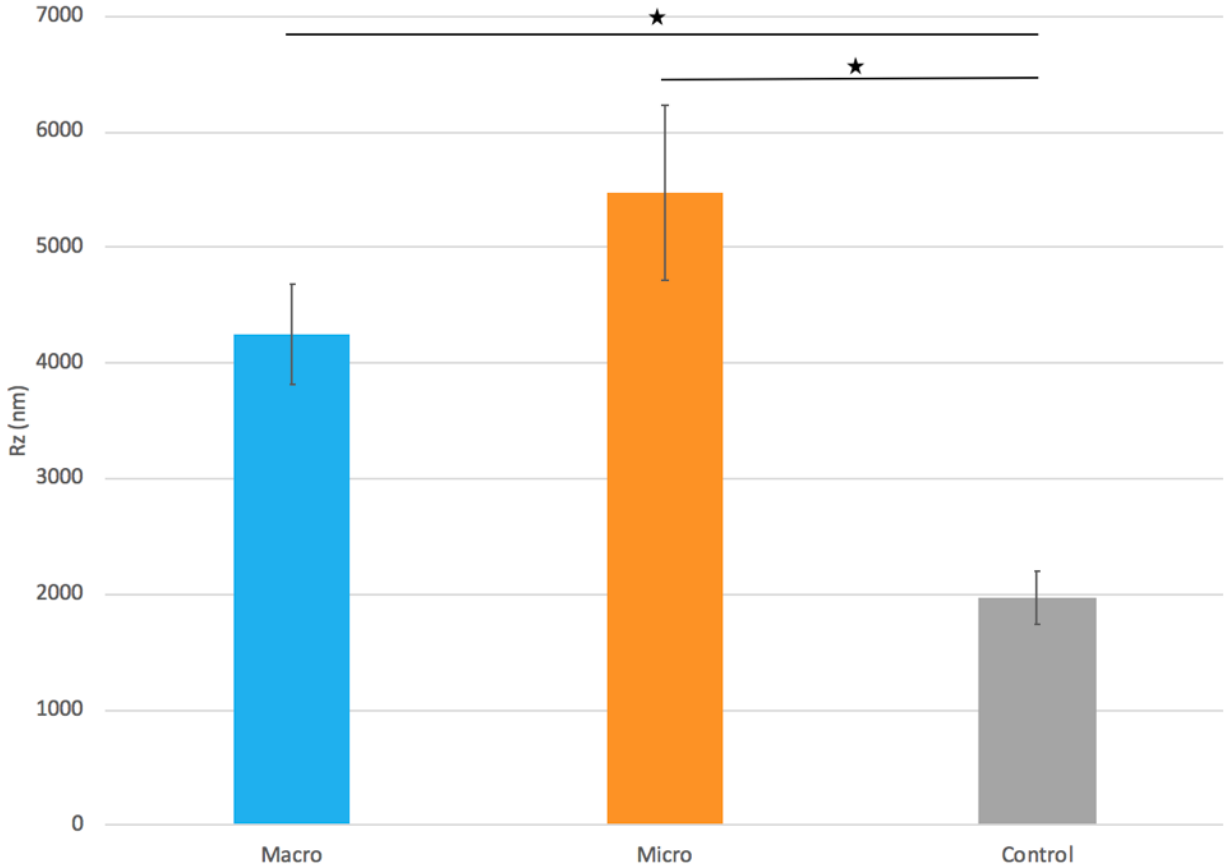


**Figure 38. Comparing average Rz values between macroscopic and microscopic deposits and a control sac. Error bars indicate the standard error of the mean.**

Two-factor t-tests ( $\alpha=0.05$ ) were conducted to determine the significance of these findings. The differences between the surface from the macroscopic deposits and the surface from the control were significant for all parameters. The differences between the surface from the microscopic deposits and the surface from the control were also significant for all parameters. The differences between the surface from the macroscopic deposits and the surface from the microscopic deposits were significant for Rq, Ra, and H.

## **Chapter 4**

### **Discussion**

#### **4.1 Summary of Findings**

This study used a method of immunofluorescently labeling platelets and fibrin to label biological deposits in the Penn State PVAD. These deposits were imaged with confocal and ESEM before biologics were degraded from the surface. Surface topography was evaluated with optical profilometry. These methods were correlated to understand the relationship between thrombosis and surface roughness. This explanted sac protocol was conducted on 13 blood sacs from ovine trials at the Penn State Hershey Medical Center. Across all 13 sacs, there were 7 macroscopic deposits and 32 microscopic deposits found.

Topography differences between samples with macroscopic and microscopic deposits and a control sac were considered to understand the surface roughness near different sizes of deposition. There was greater sac surface roughness in regions of larger thrombus deposition. The majority of the deposits were found in the transition from the inlet and outlet ports to the main body of the sac. The surface roughness parameters are higher for macroscopic and microscopic clots than for the control samples. Areas of higher roughness could promote deposition of platelets and fibrin on the surface of the SPEUU blood sacs.

#### 4.1.1 Roughness Analysis

The root mean squared ( $R_q$ ), an average deviation from the roughness average center line, the roughness average ( $R_a$ ), an average of all values on the roughness profile, the ten-point-height ( $R_z$ ), an average of the five highest peaks and the five lowest valleys, and the Swedish height ( $H$ ), a roughness average of the middle 90% of the data, were collected for each sample to characterize surface roughness. A similar trend was observed for the  $R_q$ ,  $R_a$ , and  $H$  with macroscopic deposit surfaces showing greater roughness values, microscopic deposit surfaces showing moderate roughness, and control surfaces showing low roughness. The differences in  $R_q$ ,  $R_a$ , and  $H$  values for these three types of surface were all significant. The  $R_q$  and the  $R_a$  are averages from the center line and from all values of the surface, respectively, making them both useful parameters for investigating the overall roughness of a sample. The  $H$  includes only the middle 90% of the data, which is useful in case there is debris or foreign substance on the surface that was not masked out, because this parameter prevents the data from being skewed by a few extreme points on the topography. For the  $R_z$ , the highest roughness values were observed for the surface of the microscopic deposits, followed by the surface for macroscopic deposits, then the control surface. The profilometry images for the macroscopic deposits required masking to remove residual biologics from the data. It is possible that if the biologics would have fully degraded, the  $R_z$  values would have been much higher for the macroscopic surfaces. The microscopic deposits were fully degraded, so the true surface was observed. The  $R_z$  accounted for the roughness directly under the microscopic deposits, which could be why the values for the microscopic deposits were higher. The  $R_z$  only accounts for the five highest peaks and five lowest valleys, so it should be used critically because it is easily skewed by extreme points on the topography.

### **4.1.2 Macroscopic Deposits**

The macroscopic deposits provided the most initial concern because these large regions of platelet adhesion could potentially break off and embolize, causing major complications in the body. Interestingly, none of the macroscopic deposits fully degraded from the surface of the blood sac, even after undergoing the pepsin degradation multiple times. This showed that the macroscopic deposits were quite difficult to remove from the surface. The possibility remains for small pieces of the macroscopic deposit to break off, but this study demonstrated that it would be unlikely for the entire deposit to cause an embolism. The failure of the macroscopic deposits to fully degrade created limitations for fully understanding the surface roughness under these deposits. If the true surface under these macroscopic deposits could be fully examined, it is expected that the surface roughness values would increase in those areas.

### **4.1.3 Microscopic Deposits**

While the microscopic deposits were initially a secondary concern due to their small size, the study showed that all microscopic deposits were removed from the surface with the pepsin degradation. This demonstrates that the microscopic deposits were more easily removed, making them more likely to break off and embolize, which presents more significant reason for concern. For regions with microscopic deposits, the true surface was observed due to the removal of the residual biologics. The relationship between the roughness data for the microscopic regions and the control surfaces provides valuable information because the roughness data is accurate to the true surface.

## 4.2 *In Vivo* Study Correlation

While surface topography could promote deposition on the surface of the Penn State PVAD blood sacs, factors related to the animal studies could also influence thrombosis. The animal study information describes the anticoagulation, study duration, pre-implant sac analysis, and the overall animal performance. Table 15 shows the summary of anticoagulation protocol used and study duration for each blood sac. The macroscopic deposits were found on the ovine trials with a longer study duration. In the ovine trials, two different anticoagulant protocols were used. These protocols were based on the TEG R-time. TEG is a measure of platelet function, clot strength, and fibrinolysis, and R-time is a measure of the period between the test initiation, and the initial fibrin formation. (24) The anticoagulant was either R-time 2x the normal (2R) or R-time 1x the normal (1R). Of the five blood sacs that showed macroscopic deposition, three sacs used 2R and two sacs used 1R, making the anticoagulant unlikely to have a large impact on thrombosis in these ovine trials.

**Table 15. Animal Study Statistics from the Penn State Hershey Medical Center. Macroscopic deposit locations are highlighted.**

<b>Sac Number</b>	<b>Study Duration (days)</b>	<b>Anticoagulant</b>
151	35	2R
170	77	2R
172	27	2R
176	50	2R
183	73	2R
190	63	1R
192	0	2R
223	62	2R
232	58	1R
234	62	1R
240	64	1R
247	43	1R
249	58	1R

All blood sacs were analyzed before implantation to assess surface defects. Many of the blood sacs had scuffing or scratching on the surface. The sacs that had macroscopic deposition had some of the larger and longer scuffs and scratches. Each sac was analyzed macroscopically following the explantation of the PVAD. Some deposits were visualized on the sacs prior to fixing and shipment to University Park for more thorough analysis. The blood sacs were not studied comprehensively through the explanted sac analysis at University Park, so some of these deposits could have been missed because blood sac samples were not taken in exactly the same areas as they were described in the macroscopic analysis from the Penn State Hershey Medical Center. Explanted sac sampling locations were chosen based on the macroscopic analysis provided, so it is expected that most of the deposits were studied during the explanted sac analysis. Another possibility is that deposits noted during the macroscopic analysis at the Hershey Medical Center could have been cleaned off during the sac preparation protocol following the blood sac

explantation. The sacs that were clean showed little or no deposition among the samples taken. Overall, the animal performances were good. However, Sac 170 showed that infection could be a factor contributing to thrombosis.

**Table 16. Qualitative Summary of Animal Studies from the Penn State Hershey Medical Center. Macroscopic deposit locations are highlighted.**

<b>Sac Number</b>	<b>Macroscopic Analysis</b>	<b>Pre-Implant Sac Analysis</b>	<b>Overall Animal Performance</b>
151	Clean	-	-
170	Several deposits around entire ring where diaphragm side meets stationary portion	Bubbles within SPEUU in between ports 0.75 in scuffs	Infection, many thrombi throughout the device and animal
172	Small white spot on inlet, lower diaphragm region	0.5 in scuffs 0.5 in scratches	Good
176	Clean	0.25 in scuffs near ports on diaphragm side	Good
183	White deposit on outlet side of ridge	1.5 in scratches on stationary side and inlet port 1 in scuffs on diaphragm side Bubble at inlet port	Good
190	Tiny white deposit on outside of ridge	-	Good
192	Several areas of discoloration on ridge	-	Early death
223	White deposit on ridge of the inlet and outlet	2.5 in scratches on stationary side 2.5 in scuffs on outlet side and center front diaphragm	Good

Sac Number	Macroscopic Analysis	Pre-Implant Sac Analysis	Overall Animal Performance
		Bubbles in between ports	
232	-	1.5 in scratches 0.25 in scuffs mild under inlet port on diaphragm side, worst on stationary side	Good
234	2 tiny deposits on outlet ridge and at bottom inlet side diaphragm region	1.5 in scratches under inlet port 0.5 in scuffs on stationary side	Good
240	A very faint deposit in the lower center belly section of the sac.	-	-
247	Perfectly clean	1 in scratches 1 in scuffs on center front of diaphragm side and stationary side	Early termination due to valve problem causing GI bleeding and low hematocrit
249	Larger white-reddish deposit on outlet ridge	1 in scuffs under outlet port and on stationary side	Good

### 4.3 Limitations and Future Studies

This study successfully investigated the relationship between thrombosis and surface roughness in the Penn State PVAD. The main limitation of the study was that some of the macroscopic deposits did not fully degrade, even after repeated degradation. The residual biologics blocked the analysis of the true surface of the material in those macroscopic regions. Another limitation is that only twelve regions of the blood sac were analyzed. This study expanded on the

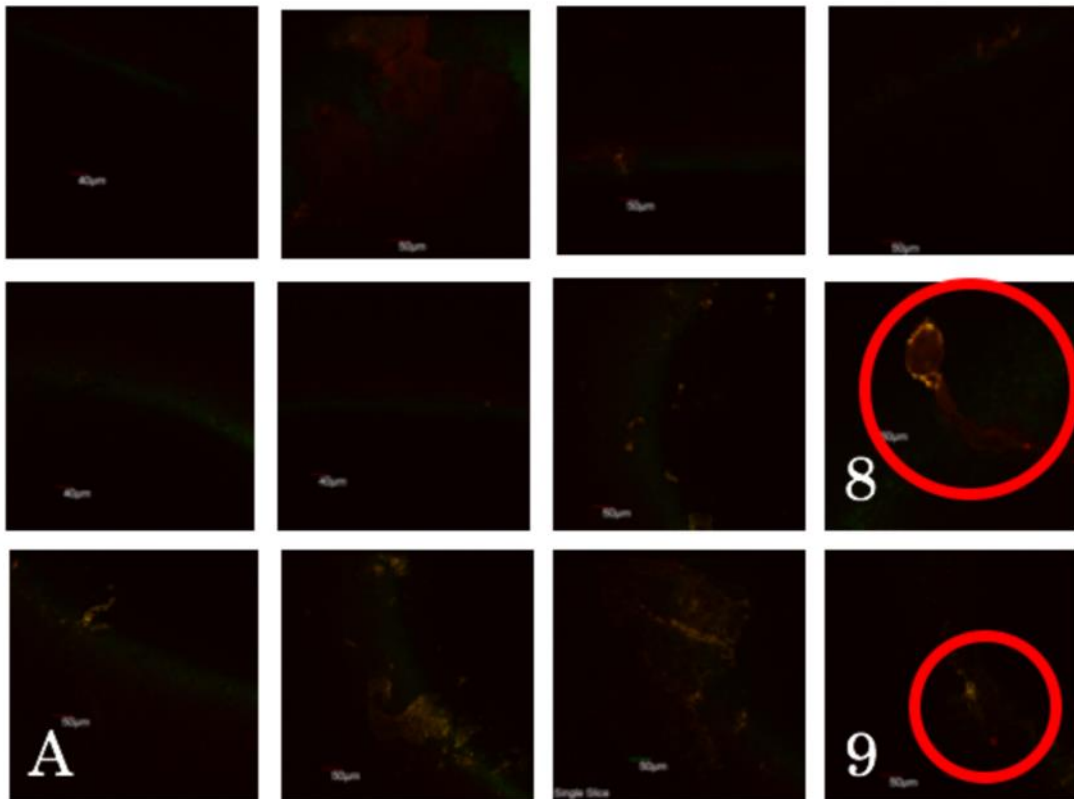
previous analysis, but further study on additional regions would provide a more thorough characterization of platelet adhesion and surface roughness of the blood sac.

A potential future study could replicate the ovine trials in a more controlled environment. This would eliminate the animal study variables and provide a more precise analysis of thrombosis, because any platelet adhesion would result from either fluid flow or surface defects. These controlled studies could also incorporate intentional surface defects to investigate how different types of scratches and scuffing are related to thrombosis.

Overall, this study provides a protocol for studying the relationship between thrombosis and surface roughness on the SPEUU blood sacs. This protocol can be applied to future studies to understand how the SPEUU material functions in the design of other mechanical circulatory support devices.

## Appendix A

### Additional Correlated Images of Macroscopic Deposits



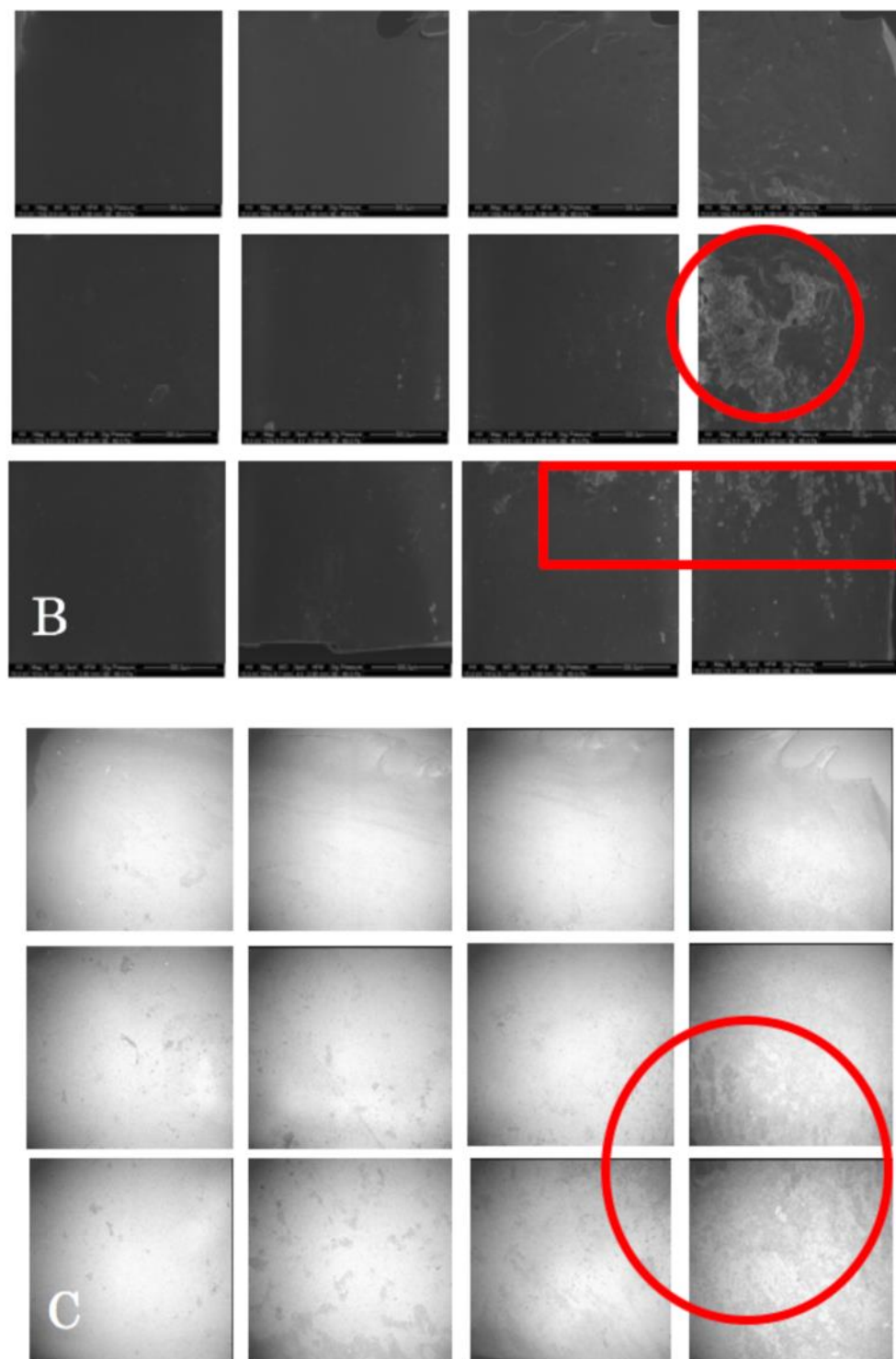


**Figure 39. A small, macroscopic deposit found with (A) confocal, was confirmed with (B) ESEM at the inlet of Sac 170. The (C) profilometry showed scuffing. (34)**

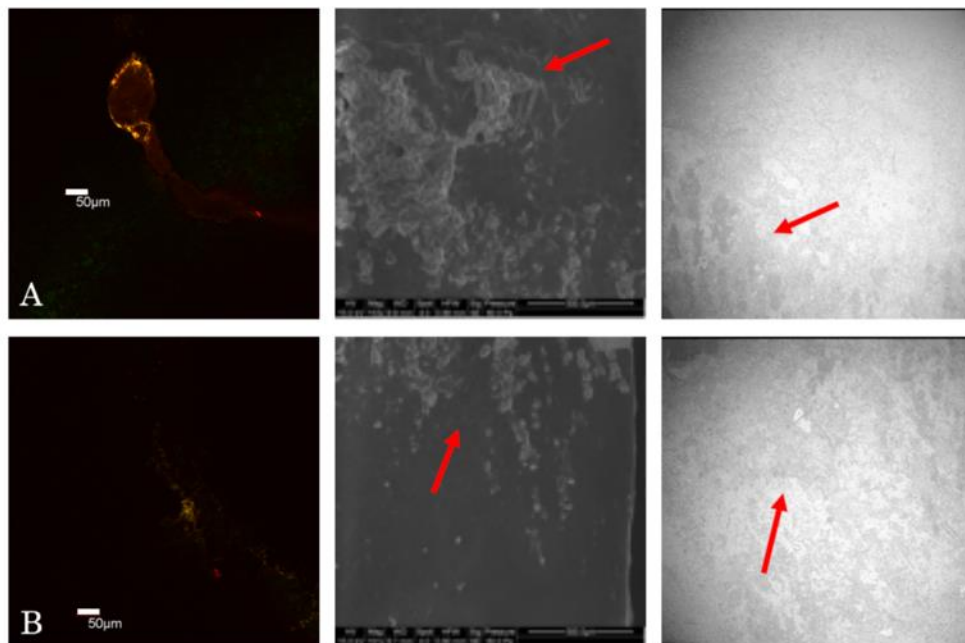
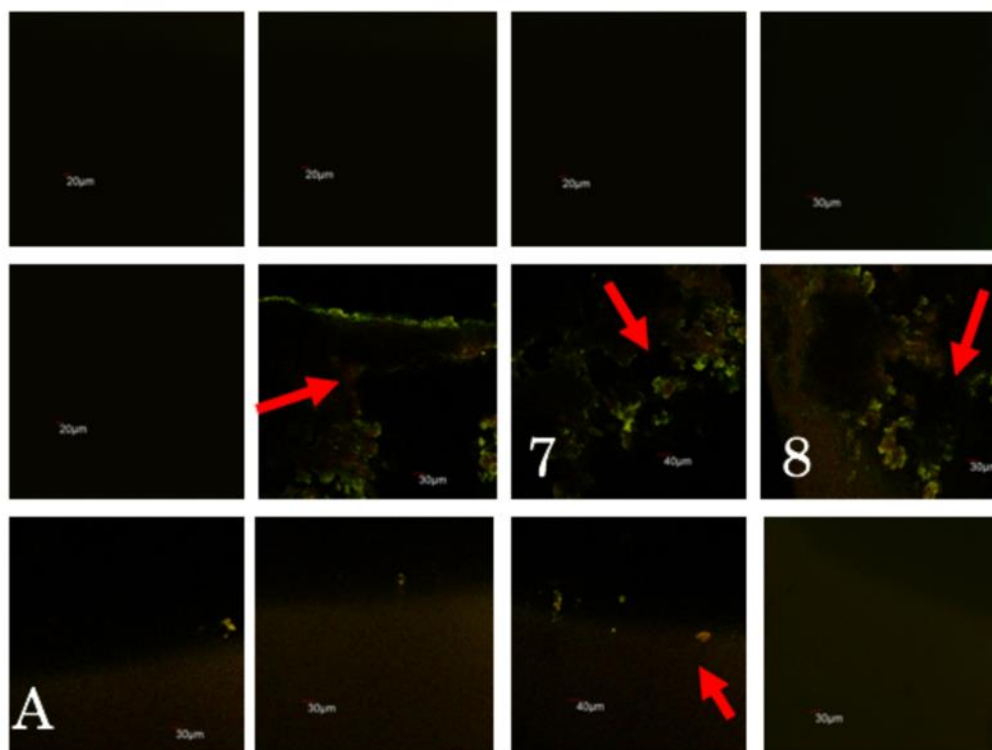
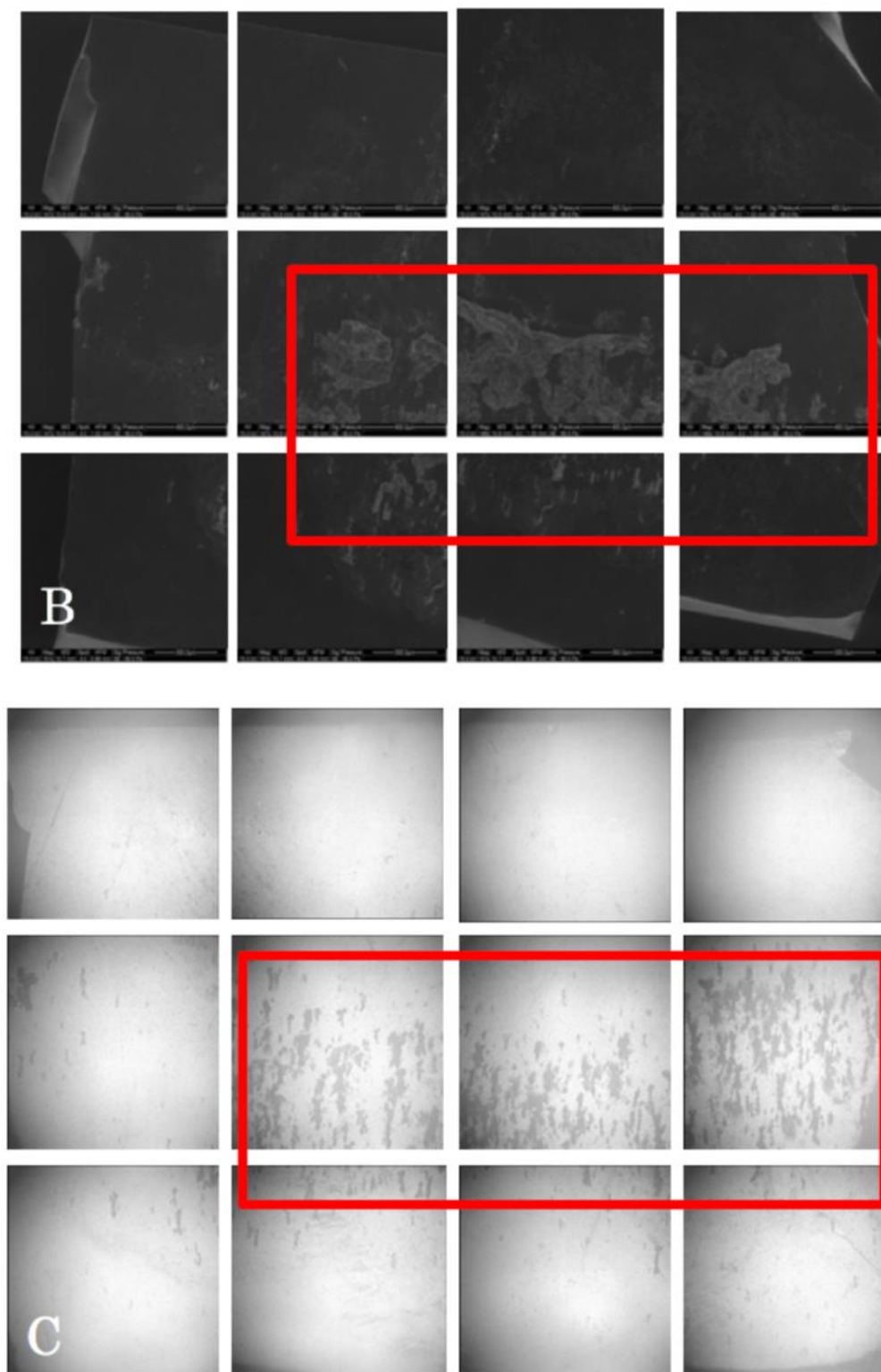


Figure 40. A closer examination of (A) Region 8 and (B) Region 9 of the inlet of Sac 170.  
(34)





**Figure 41. A large, macroscopic deposit found with (A) confocal and confirmed with (B) ESEM. Residual biologics are seen on (C) the profilometry of the inlet of Sac 183. (34)**

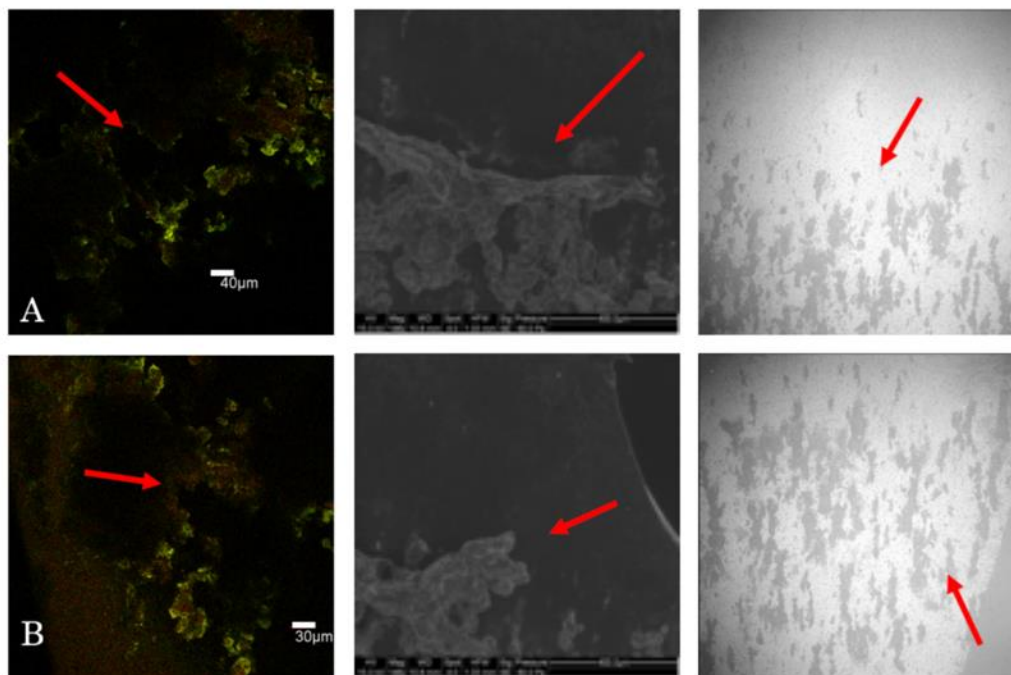
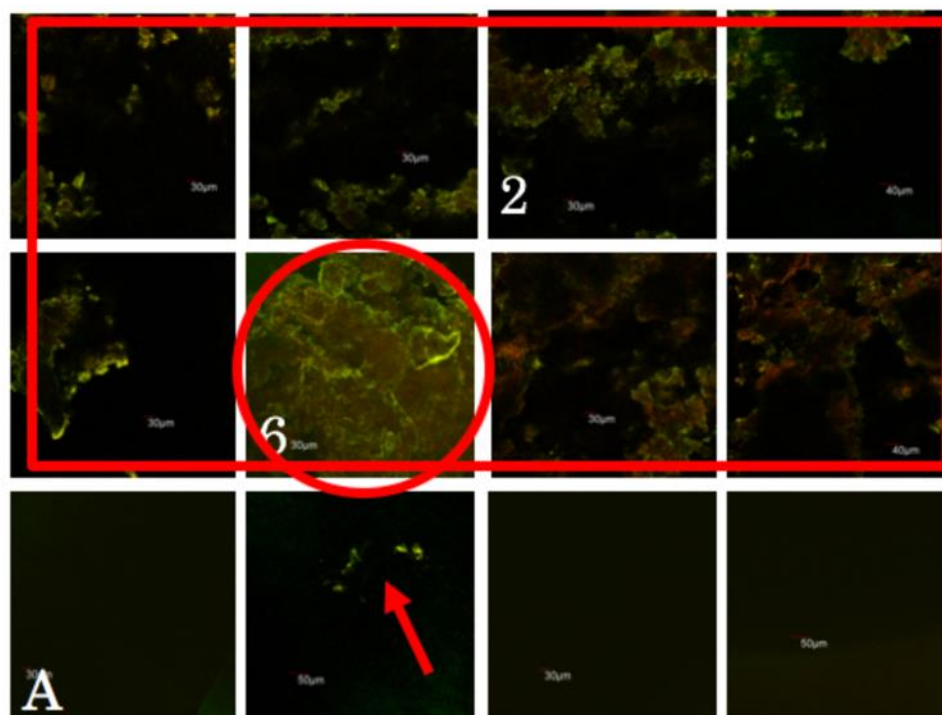
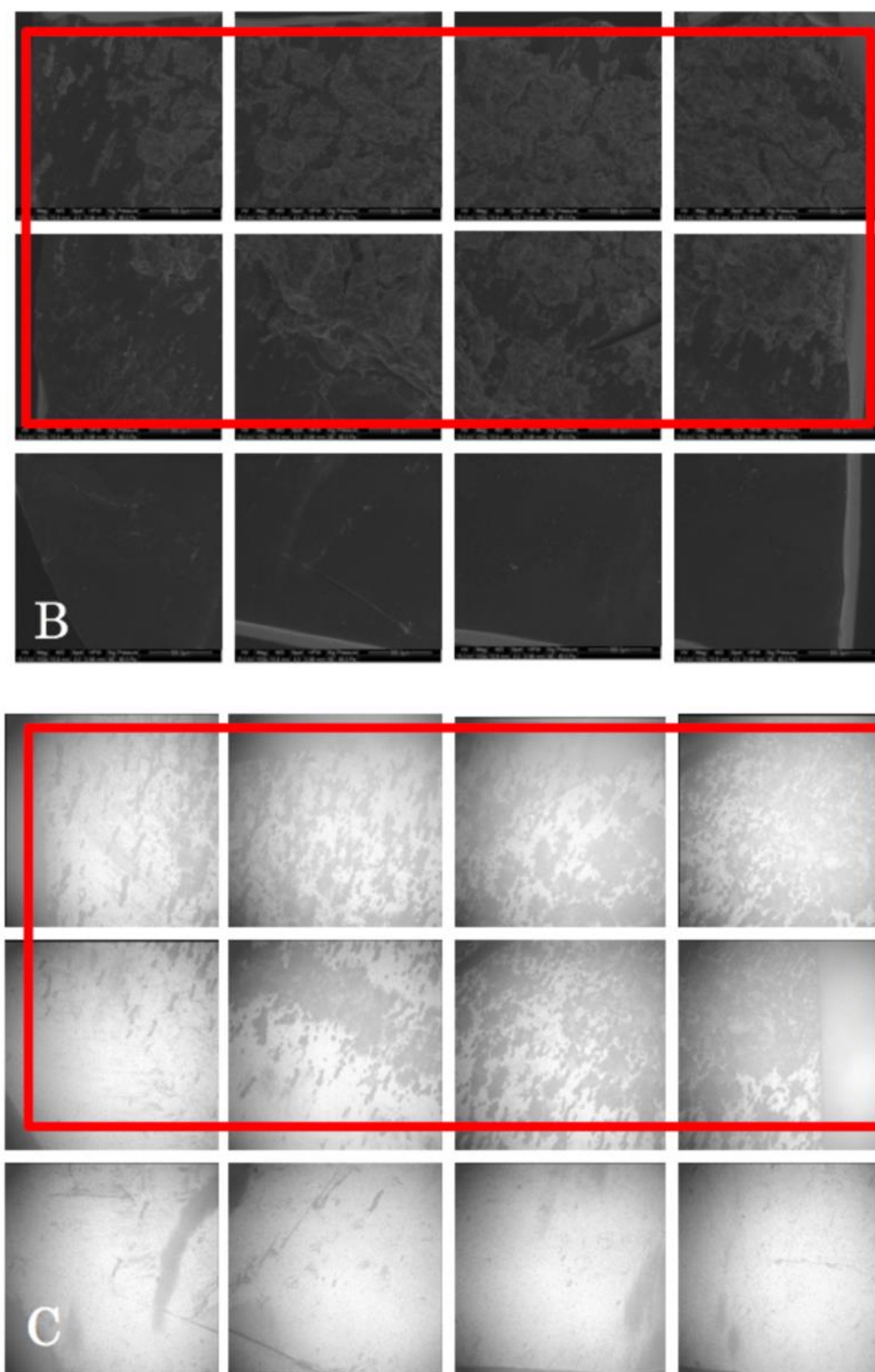


Figure 42. A closer examination of (A) Region 7 and (B) Region 8 of the inlet of Sac 183.  
(34)





**Figure 43. A very large macroscopic deposit seen by (A) confocal and (B) ESEM on the outlet of Sac 183. The (C) profilometry shows residual biologics on the surface. (34)**

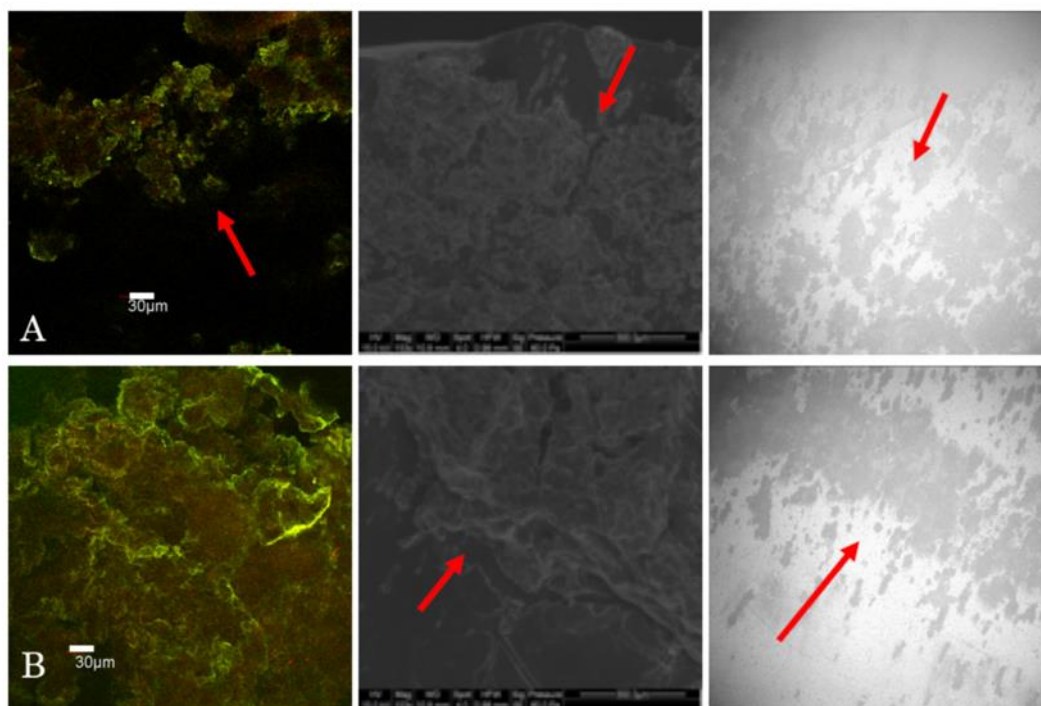
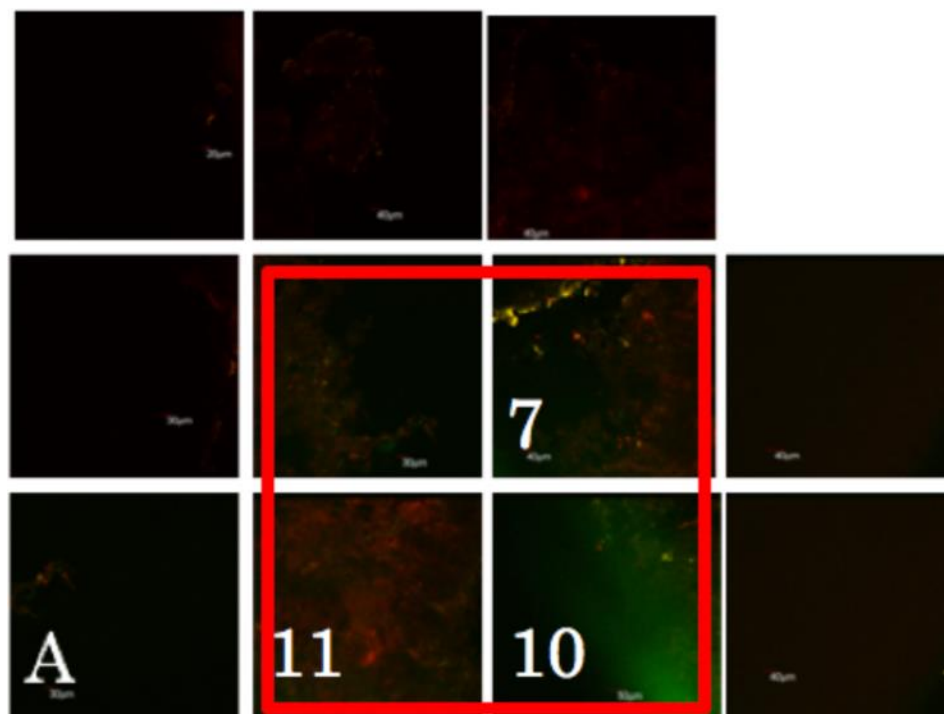
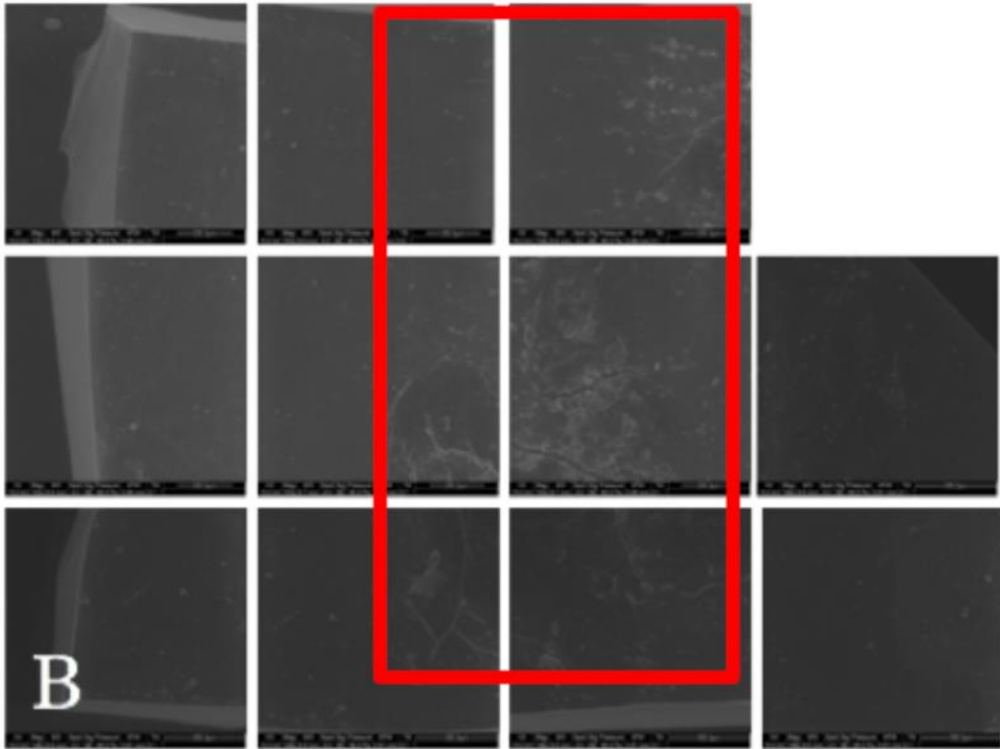
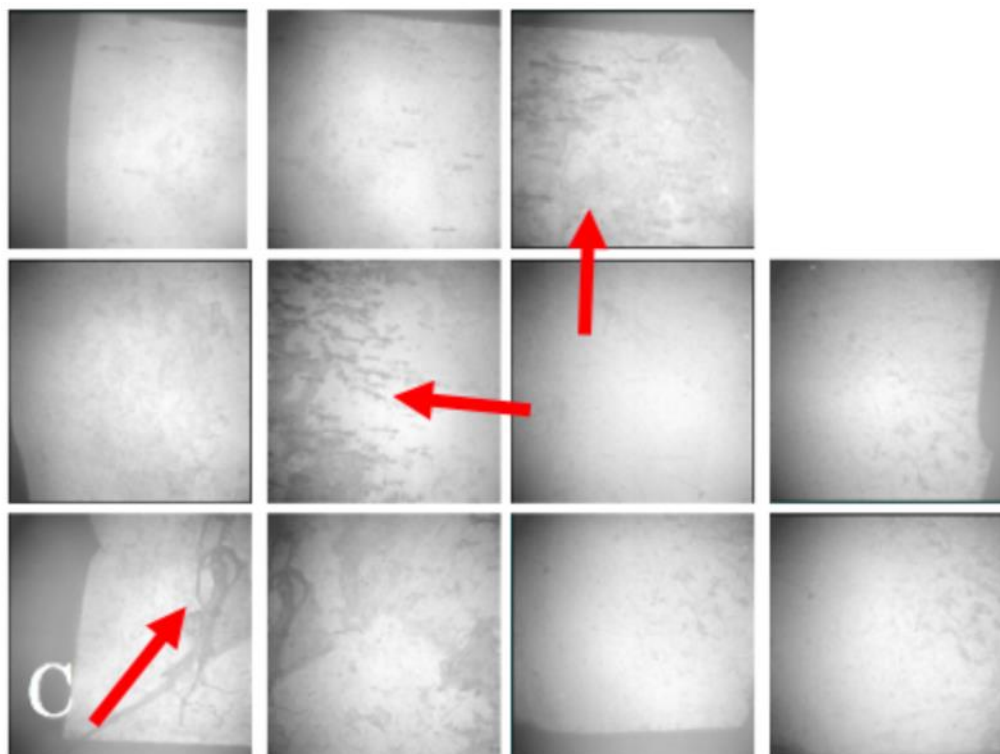


Figure 44. A closer examination of (A) Region 2 and (B) Region 6 of the outlet of Sac 183.  
(34)







**Figure 45. A large, macroscopic deposit shown by (A) confocal and (B) ESEM. There are residual biologics on (C) the profilometry image of the outlet of Sac 190. (34)**

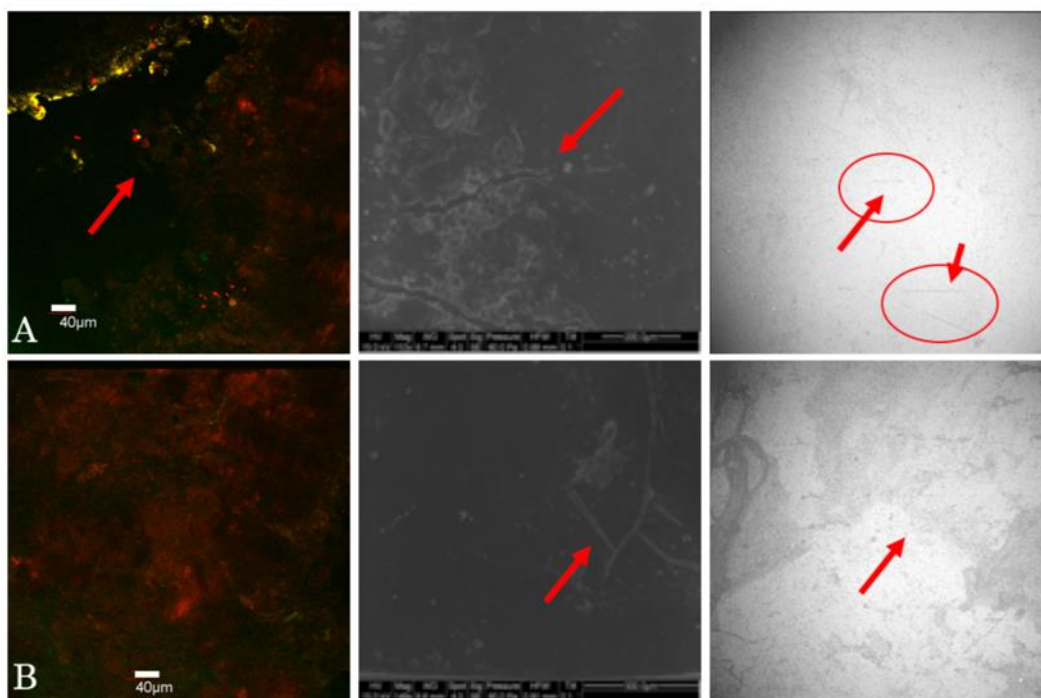
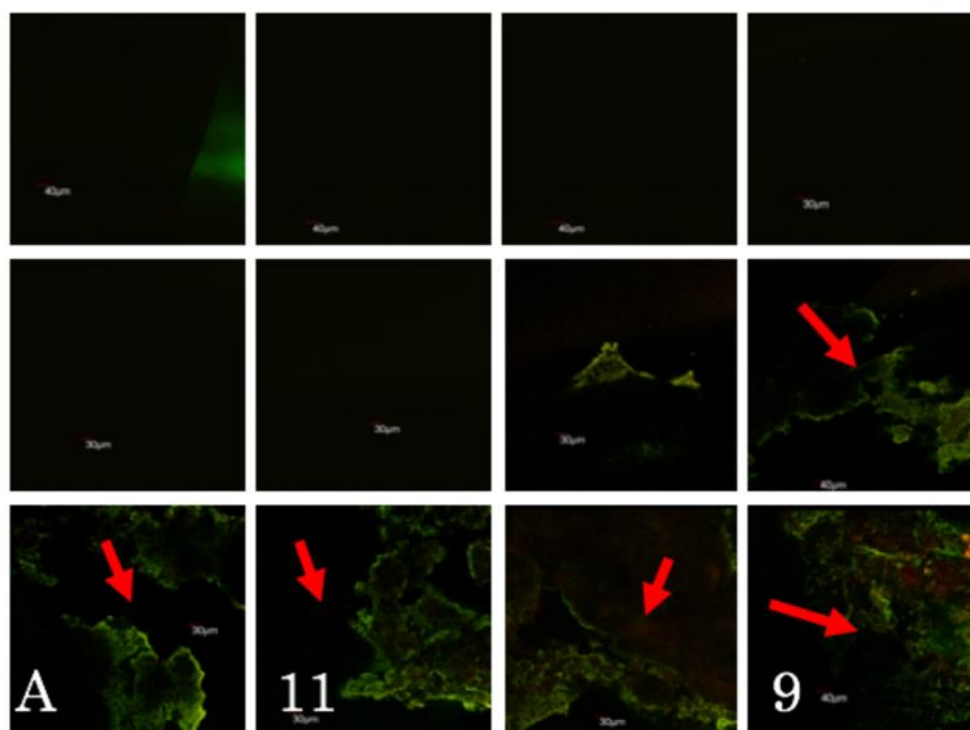
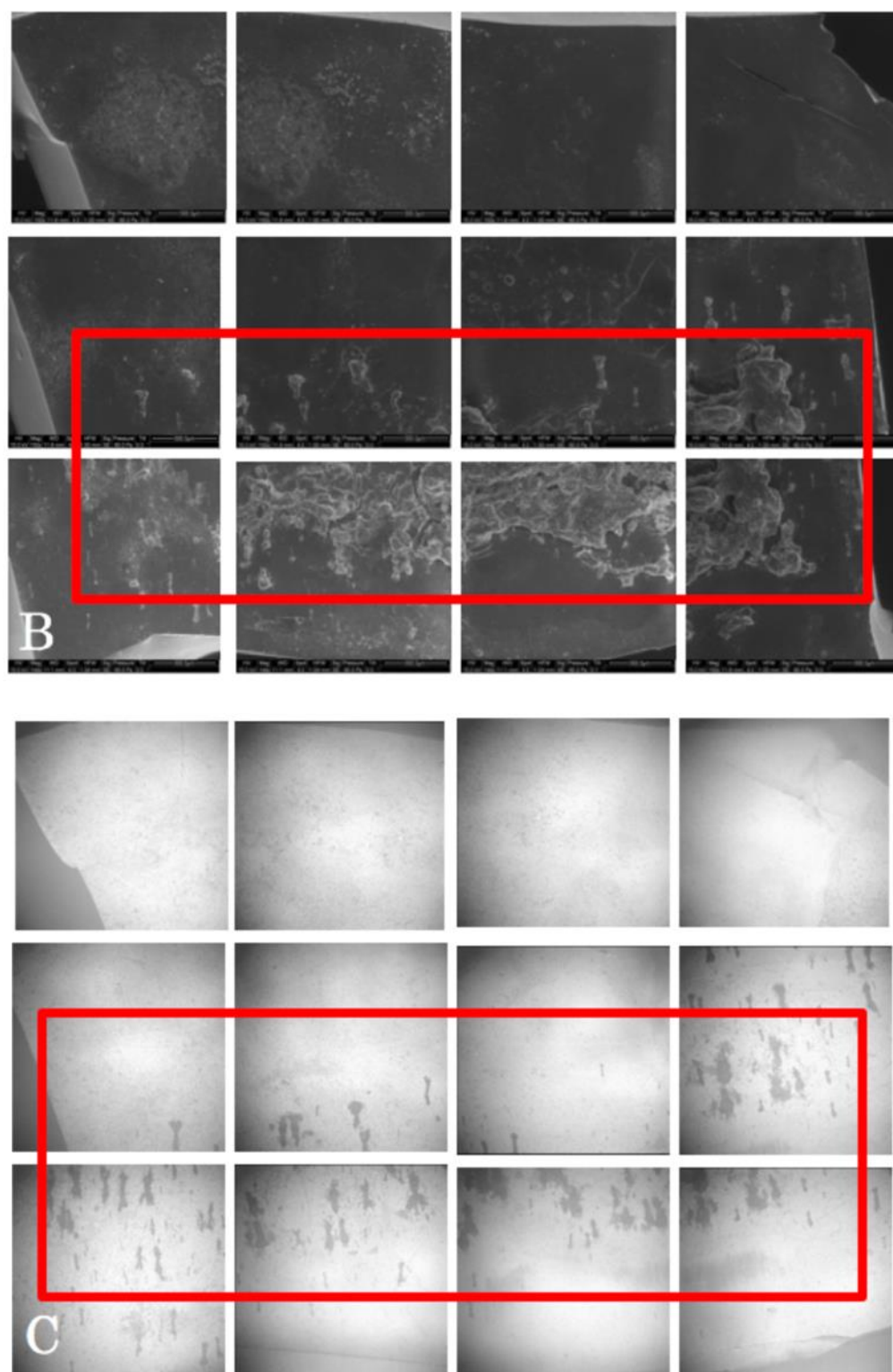
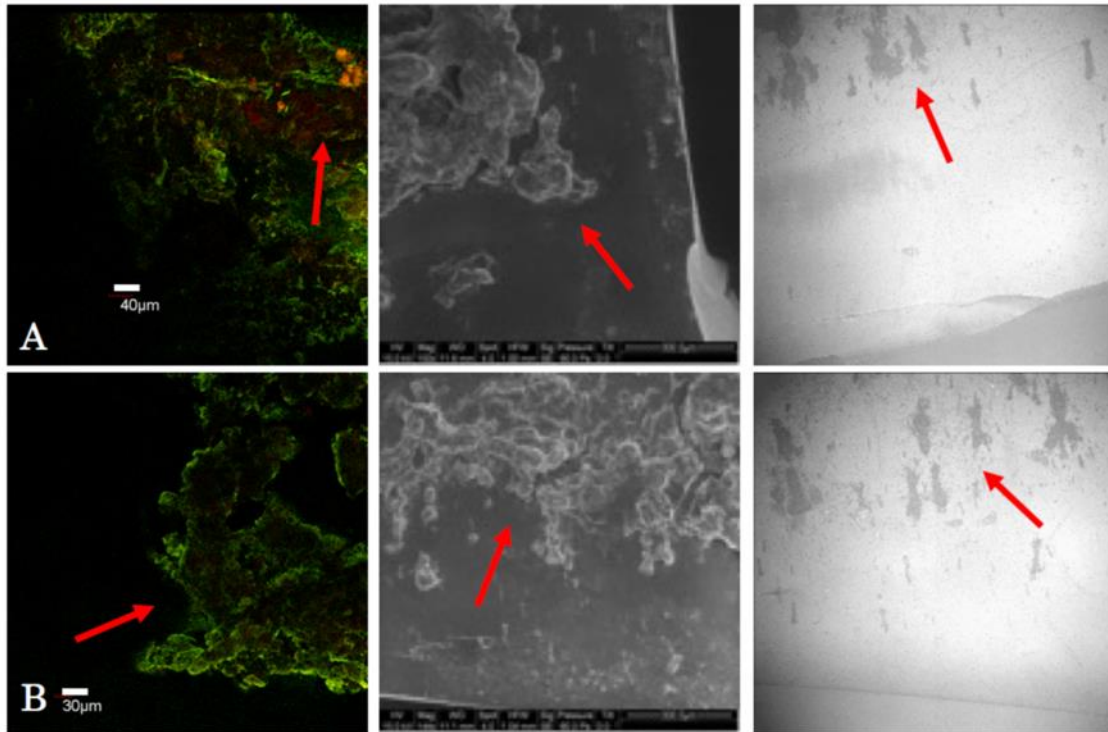


Figure 46. A closer examination of (A) Region 7 and (B) Region 11 of the outlet of Sac 190.  
(34)





**Figure 47. A dense, macroscopic deposit shown by (A) confocal and (B) ESEM. The (C) profilometry shows residual biologics on the outlet of Sac 234. (34)**



**Figure 48. A closer examination of (A) Region 9 and (B) Region 11 of the outlet of Sac 234.  
(34)**

## Appendix B

### Additional Correlated Images of Microscopic Deposits

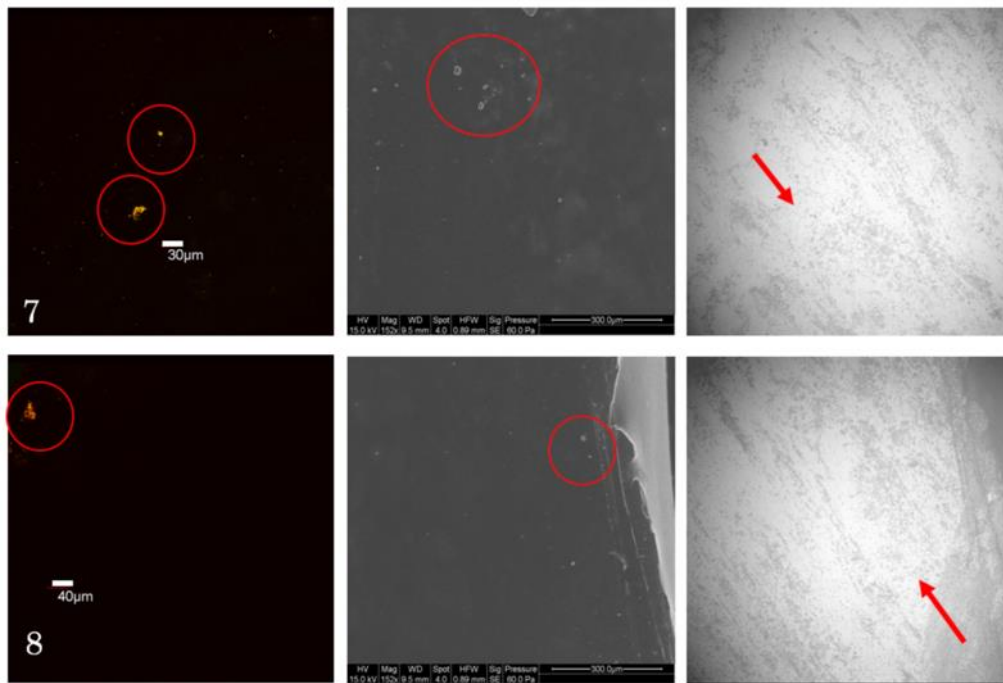


**Figure 49. Small deposits found on confocal and ESEM with the topography showing a scuffed surface on the center front of Sac 170. (A) Region 7 and (B) Region 8 are highlighted. (34)**

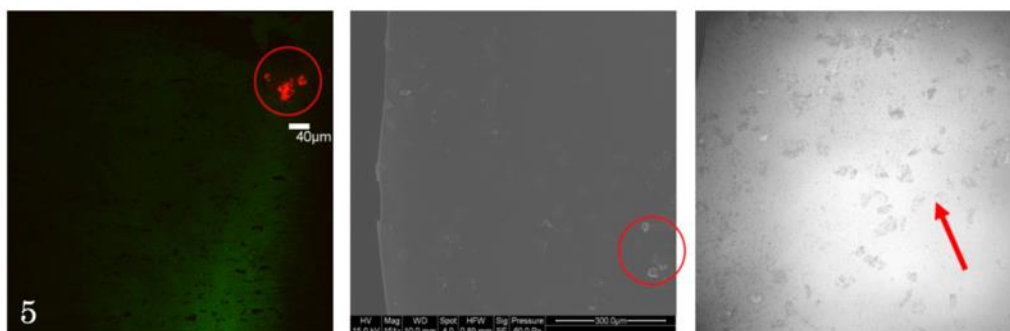


**Figure 50. A small deposit shown by confocal and ESEM at Region 5 on the inlet side of Sac 172. The profilometry image shows debris on the surface. (34)**



**Figure 51. A small deposit shown by confocal and ESEM on Region 2 of the inlet of Sac 176. The profilometry shows a smooth surface. (34)**

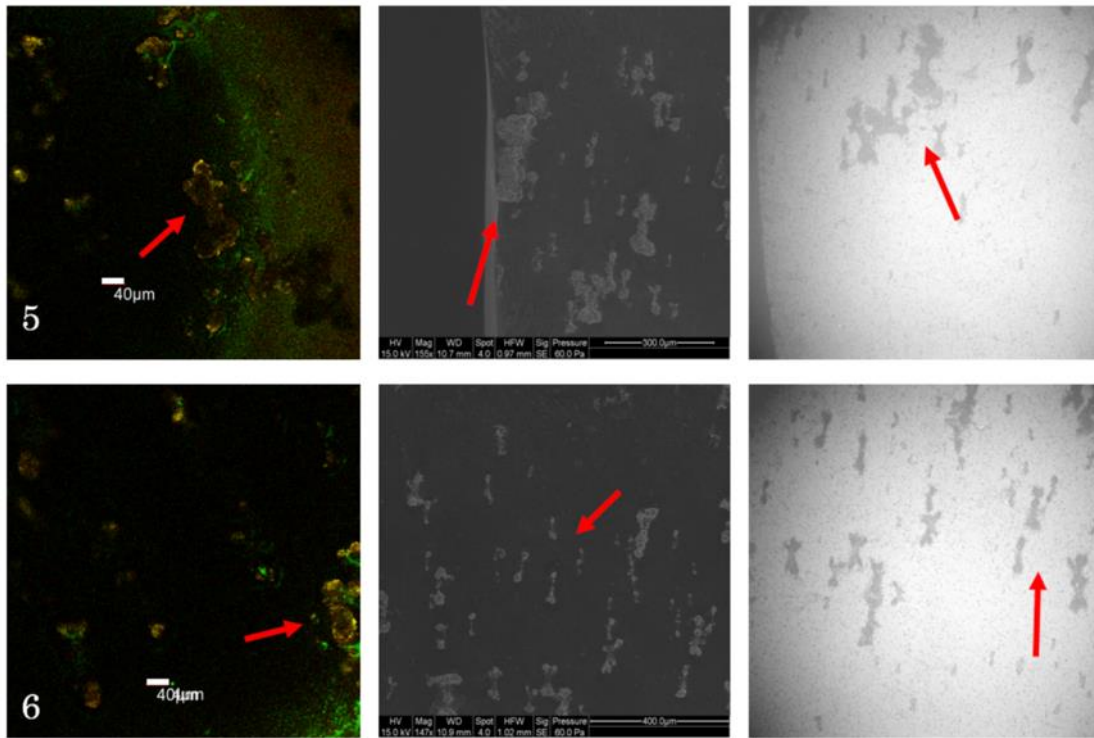


**Figure 52. A large, microscopic deposit was shown by confocal and ESEM on Regions 5 and 6 of the outlet side of Sac 183. The profilometry shows residual biologics. (34)**

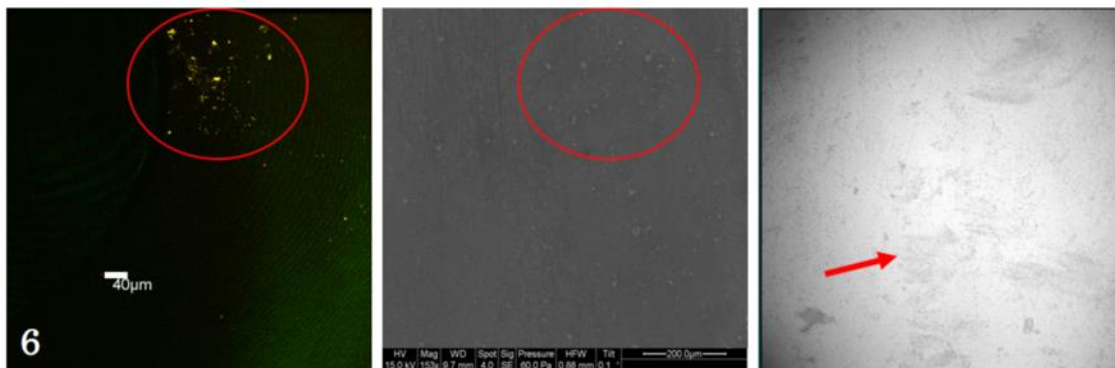


**Figure 53. Yellow, microscopic deposits are shown by confocal and confirmed by ESEM on Region 6 of the center back of Sac 190. The profilometry shows some scuffing on the topography. (34)**

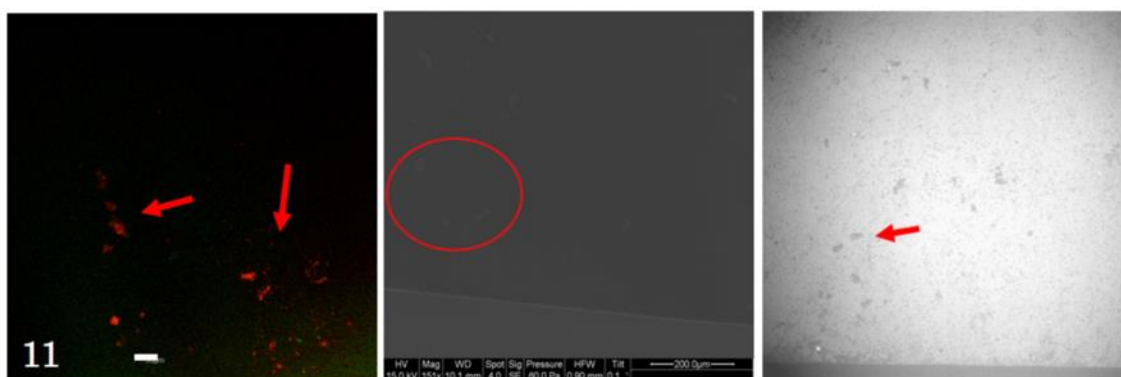


Figure 54. Red deposits are shown by confocal and seen faintly with ESEM on Region 11 of the center back of Sac 192. The topography shows some debris or pitting. (34)

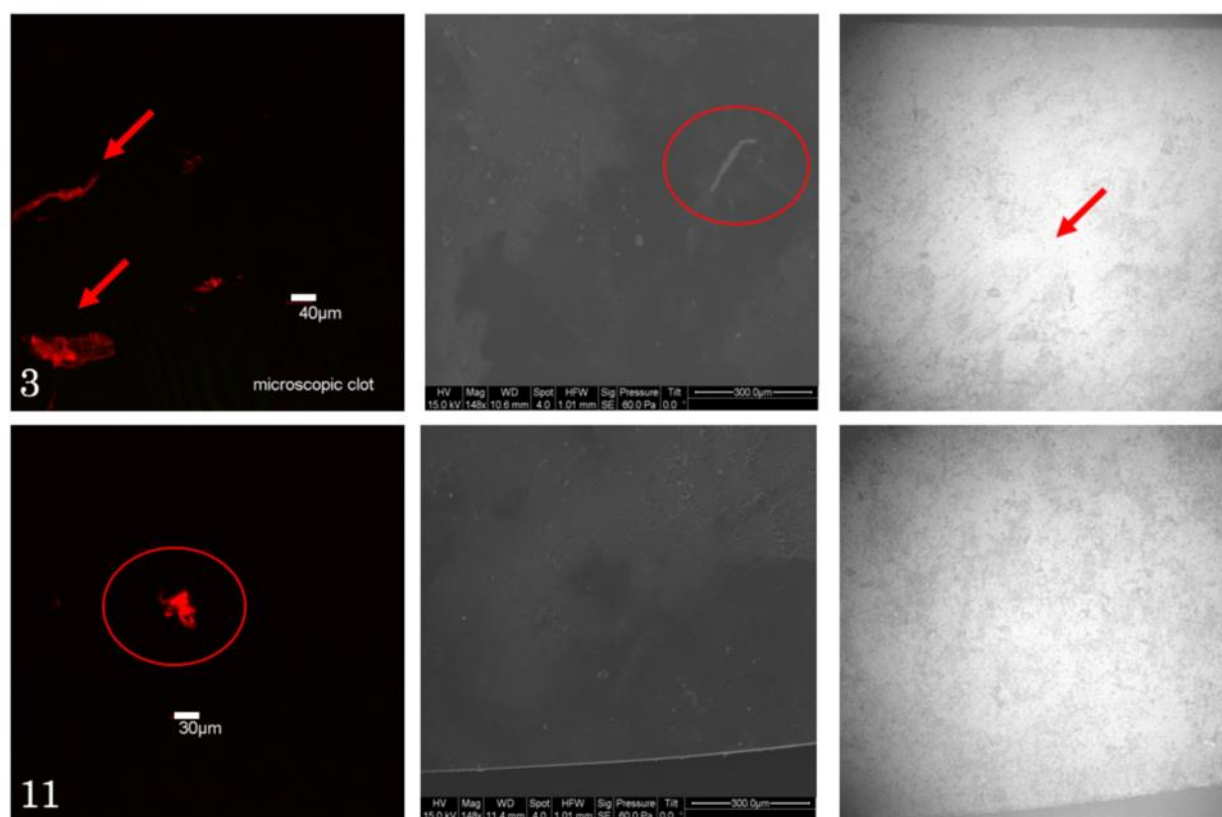


Figure 55. Large, microscopic deposits are shown on confocal and seen faintly on ESEM in Regions 3 and 11 of the top sample of Sac 223. A rougher surface is observed from the profilometry images. (34)

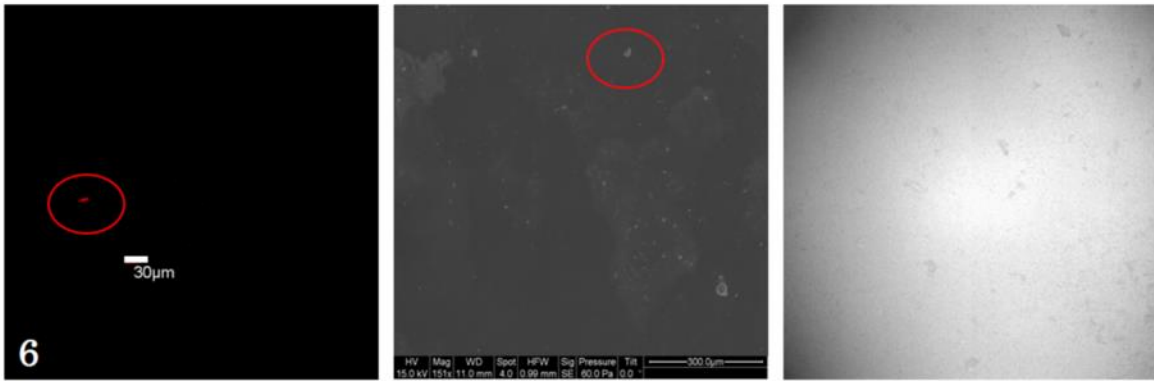


Figure 56. A small, microscopic deposit shown on confocal and confirmed with ESEM on Region of the outlet of Sac 232. The profilometry shows a smooth surface. (34)

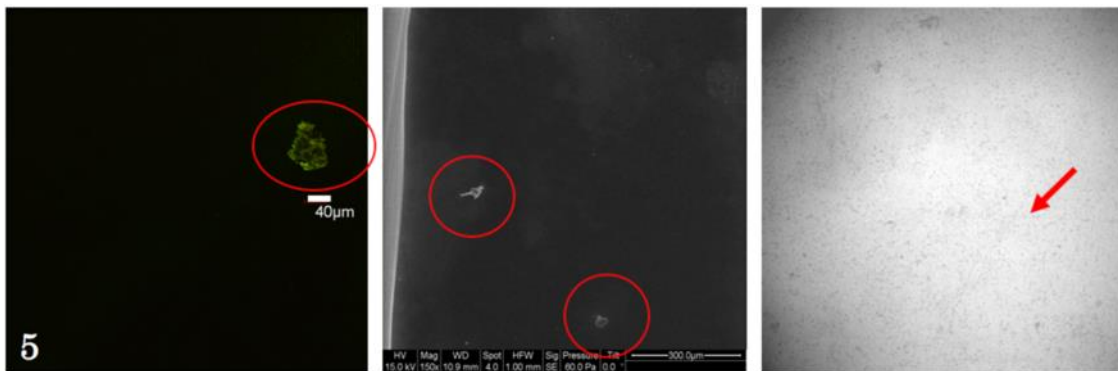
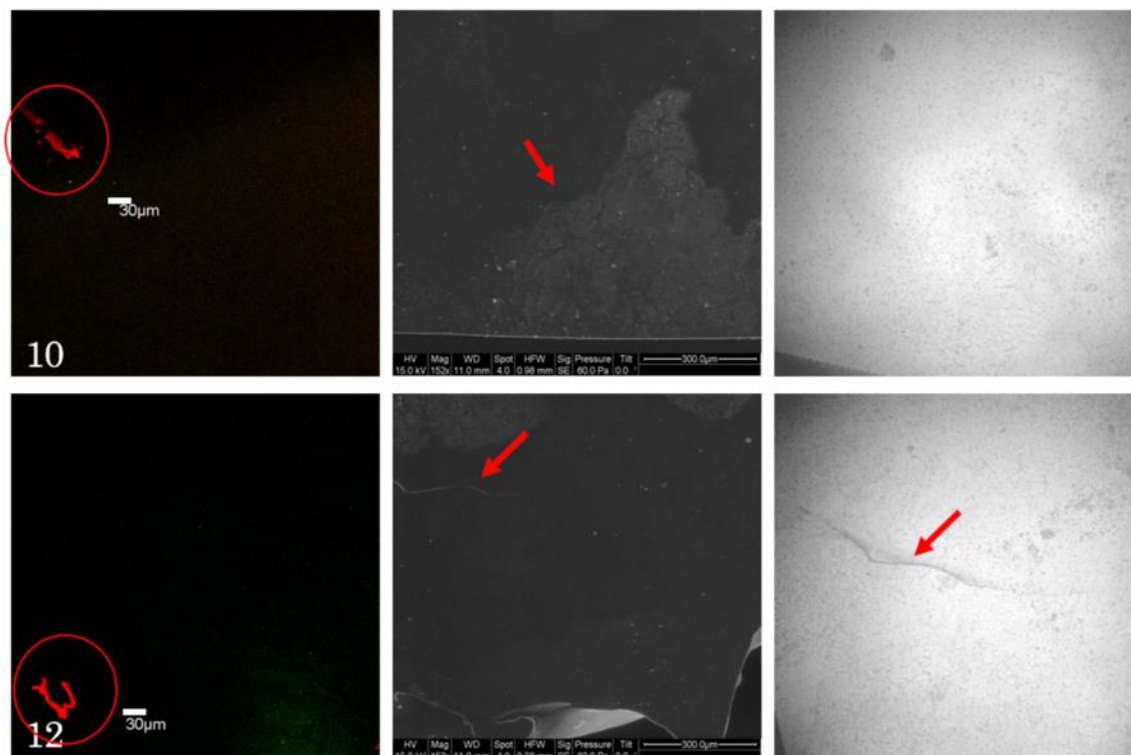
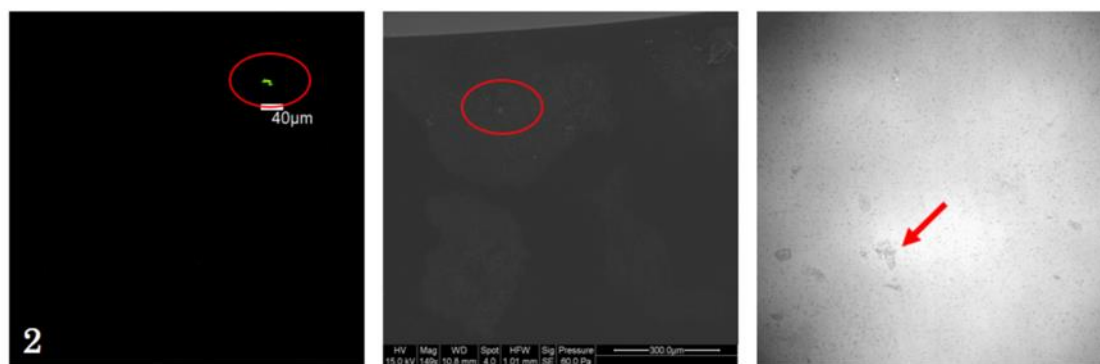


Figure 57. A deposit shown by confocal and confirmed by ESEM on Region 5 of the center front of Sac 234. The red arrow points to a scratch shown on the profilometry image. (34)



**Figure 58. Red deposits shown by confocal and ESEM on Regions 10 and 12 of the top sample of Sac 247. A divot is shown on the ESEM and profilometry of Region 12. (34)**



**Figure 59. A small, green deposit is shown on confocal and confirmed with ESEM. The red arrow points to debris on the topography of the profilometry image. (34)**

## BIBLIOGRAPHY

- (1) Organ Procurement and Transplantation Network. US Department of Health and Human Services: Health Resources and Services Administration. <https://optn.transplant.hrsa.gov/>
- (2) World Health Organization. Cardiovascular diseases. [http://www.who.int/news-room/fact-sheets/detail/cardiovascular-diseases-\(cvds\)](http://www.who.int/news-room/fact-sheets/detail/cardiovascular-diseases-(cvds))
- (3) Benjamin EJ, et al.: Heart Disease and Stroke Statistics – 2017 Update: A Report from the American Heart Association. *Circulation*. 135, e146-e603, 2017.
- (4) Tonsho M, et al.: Heart Transplantation: Challenges Facing the Field. *Cold Spring Harbor*. 1-21, 2014.
- (5) Gilboa SM: Congenital Heart Defects in the United States. *Circulation*. 134, 101-109, 2016.
- (6) Lee TM: Pediatric Cardiomyopathies. *Circulation Research*. 121, 855-873, 2017.
- (7) Jayaprasad N: Heart Failure in Children. *Heart Views*. 17, 92-99, 2016.
- (8) Organ Procurement and Transplantation Network. US Department of Health and Human Services: Health Resources and Services Administration. <https://optn.transplant.hrsa.gov/>
- (9) Helman D, Rose EA: History of mechanical circulatory support. *Progress in Cardiovascular Diseases*. 43, 1-4, 2000.
- (10) Kozik D, Plunkett M: Mechanical Circulatory Support. *Organogenesis*. 7, 50-63, 2011.
- (11) Rodriguez LE, et al.: Ventricular Assist Devices (VAD) Therapy: New Technology, New Hope? *Methodist Debaquey Cardiovascular Journal*. 9, 32-37, 2013.

- (12) Maslach-Hubbard A, Bratton SL: Extracorporeal membrane oxygenation for pediatric respiratory failure. *WJCCM*. 2, 29-39, 2013.
- (13) Cabrera AG, et al.: Outcomes of pediatric patients supported by the HeartMate II left ventricular assist device in the United States. *J Heart Lung Transplant*. 32, 1107-1113, 2013.
- (14) Miera O, et al.: A multicenter study of the HeartWare ventricular assist device in small children. *J Heart and Lung Transplantation*. 35, 679-681, 2016.
- (15) Burki S, Adachi I: Pediatric ventricular assist devices: current challenges and future prospects. *Vasc Health Risk Manag*. 13, 177-185, 2017.
- (16) Fraser C, Jaquiss R: The Berlin Heart EXCOR Pediatric ventricular assist device: history, North American experience, and future directions. *Ann N.Y. Acad. Sci*. 1291, 96-105, 2013.
- (17) Zimpfer D, et al.: Multicentre clinical trial experience with the HeartMate3 left ventricular assist device: 30-day outcomes. *European J Cardio-Thoracic Surg*. 50, 548-554, 2016.
- (18) McGee E, et al.: *In Vivo* Evaluation of the HeartWare MVAD Pump. *J Heart and Lung Transplantation*. 33, 366-371, 2014.
- (19) Wei X, et al.: Pre-clinical evaluation of the infant Jarvik 2000 heart in a neonate piglet model. *J Heart and Lung Transplantation*. 32, 112-119, 2012.
- (20) Weiss WJ, et al.: Chronic *in vivo* testing of the Penn State Pediatric Ventricular Assist Device. *ASAIO J*. 58, 65-72, 2012.
- (21) Baldwin JT, et al.: The National Heart, Lung, and Blood Institute Pediatric Circulatory Support Program. *Circulation*. 113, 147-155, 2006.

- (22) Bourassa MG, et al.: Scanning electron microscopy of surface irregularities and thrombogenesis of polyurethane and polyethylene coronary catheters. *Circulation*. 53, 992-996, 1976.
- (23) Carney EL, et al.: Animal model development for the Penn State Pediatric Ventricular Assist Device. *Artif Organs*. 33, 953-957, 2009.
- (24) Palta S, et al.: Overview of the coagulation system. *Indian J Anaesth*. 58, 515-523, 2014.
- (25) PMG Biology: Platelets and Blood Clotting *PMG Biology*. Available at: <https://pmgbiology.com/2014/06/08/platelets-and-blood-clotting-a-understanding-for-igcse-biology/> Accessed December 30, 2018.
- (26) Goldhaber SZ, et al.: Treatment of blood clots. *Circulation*. 106, e138-e140, 2002.
- (27) Burke A, Hasirci N: Polyurethanes in Biomedical Applications. *Biomaterials*. 83-101, 2004.
- (28) Yamanaka H, et al.: Multiscale Analysis of Surface Thrombosis *In Vivo* in a Left Ventricular Assist System. *ASAIO J*. 51, 567-577, 2005.
- (29) Milner KR, Snyder AJ, Siedlecki CA: Sub-micron texturing for reducing platelet adhesion to polyurethane biomaterials. *J Biomed Mater Res A*. 76: 561–70, 2006.
- (30) Hubbell JA, McIntire LV: Visualization and analysis of mural thrombogenesis on collagen, polyurethane and nylon. *Biomaterials* 7, 354–360, 1986.
- (31) Wagner WR, Schaub RD, Sorensen EN, Snyder TA, Wilhelm CR, Winowich S, Borovetz HS, Kormos RL: Blood biocompatibility analysis in the setting of ventricular assist devices. *J Biomater Sci Polym Ed*. 11: 1239-1259, 2000.
- (32) Koh LB, Rodriguez I, Venkatraman SS: The effect of topography of polymer surfaces on platelet adhesion *Biomaterials*. 31: 1533–1545, 2010.

- (33) Ceneviva N: Protocol and Initial Surface Analysis of Polymer Blood Sacs for the Penn State Pediatric Ventricular Assist Device, 2015. Penn State University, Honors Thesis.
- (34) Mueser A: Relationship of platelet adhesion with surface topography in the Penn State pediatric ventricular assist device, 2017. Penn State University, Honors Thesis.
- (35) Topper S: A correlative study of fluid mechanics and evidence of thrombus formation within the Penn State 50 cc V-2 left ventricular assist device, 2012. Penn State University, Honors Thesis.
- (36) Olympus: Introduction to Confocal Microscopy *Olympus Corporation*. Available at: <https://www.olympus-lifescience.com/en/microscope-resource/primer/techniques/confocal/confocalintro/>. Accessed December 30, 2018.
- (37) XOS: Environmental Scanning Electron Microscopy *XOS*. Available at: <https://www.xos.com/ESEM>. Accessed December 30, 2018.
- (38) Donald, A.M. The use of environmental scanning electron microscopy for imaging wet and insulating materials. *Nat Mater* 2: 511–6, 2003.
- (39) NanoScience: Optical Profilometry *NanoScience Instruments*. Available at: <https://www.nanoscience.com/techniques/optical-profilometry/>. Accessed December 30, 2018.
- (40) Zygo Corporation: Optical Profilers - How Optical Profilers Work *Zygo Metrol Bus Segm* Available at: <https://www.zygo.com/?/met/profilers/opticalprofilersabout.htm>. Accessed December 30, 2018.
- (41) Zygo Corporation: MetroPro Surface Texture Parameters *www.zygo.com*: 1–20, 2013.

- (42) Javier Conde Vancells: Direct vs indirect immunofluorescence. *Abcam*: Available at:  
<http://www.abcam.com/secondary-antibodies/direct-vs-indirectimmunofluorescence>.  
Accessed December 30, 2018.

ACADEMIC VITAE

CECILIA RICHARDSEN

EDUCATION

The Pennsylvania State University Class of 2019
Bachelor of Science in Biomedical Engineering

- Schreyer Honors College

Palmyra Area High School Class of 2015

- Valedictorian

EMS AND CLINICAL EXPERIENCE

Emergency Medical Technician Spring 2017-Present

University Ambulance Service; Assistant Chief, Crew Chief
Centre Life Link EMS; Volunteer

- Certified in American Heart Association BLS, Emergency Medical Services Vehicle Operation, HAZMAT Operations, and EMT Basic
Provided 1,500+ hours of quality care services during medical emergencies
Responded with a team to 180+ dispatched emergency assignments quickly and safely
Operated emergency vehicles in a safe manner and maintained current knowledge of treatment protocols
Implemented a student leadership structure and served as the Assistant Chief of University Ambulance Service, supervising 54 EMTs and guiding the direction of a team of officers to manage logistics, daily operations, scheduling, training, safety, and quality assurance

Job Shadowing, Penn State Hershey Medical Center Summer 2016-Summer 2017
advised by Dr. Debra Miller, M.D.

- Observed medical procedures and instruction in the internal medicine department
Shadowed 30 hours during each summer in 2016 and 2017

TEACHING EXPERIENCE

EMT Training, Adjunct Faculty Spring 2017-Present

Penn State University, KINES 403
Harrisburg Area Community College, EMT Program

- Utilized reality based scenarios, simulations, team exercises, group discussions, and lectures to prepare students for the National Registry of Emergency Medical Technicians examinations
Taught students for 100+ hours in two different EMT training classes

CPR, Instructor Spring 2017-Present

- Certified through the American Heart Association to teach basic life support, CPR, and first aid
Assessed competence, obtained feedback of understanding from students, and demonstrated effective communication based on individual learning preferences

Leadership JumpStart Program, Teaching Assistant Fall 2016-Fall 2018

- Coordinated activities and lessons for students in this 3-credit honors level course to assist students in learning leadership lessons through reflection and teamwork
Implemented semester-long service project focused on the support and promotion of local businesses through creation of a blog and organization of community events

RESEARCH EXPERIENCE

Artificial Heart and Cardiovascular Fluid Dynamics Lab Spring 2017-Present

advised by Dr. Keefe Manning, Ph.D.

- Studied the relationship between blood clotting and surface topography in pediatric heart assist devices in progress toward an honors thesis
Selected for the Summer Translational Cardiovascular Science Institute in 2018 to engage in an intensive summer program focused on cardiovascular research at Penn State University

## **ABSTRACTS AND PRESENTATIONS**

**Richardsen, C.** (June 2018). *Relationship of Platelet Adhesion with Surface Topography in the Penn State Pediatric Ventricular Assist Device*. Presented at the American Society for Artificial Internal Organs Annual Conference. Washington, D.C.

**Richardsen, C.** (April 2018). *Relationship of Platelet Adhesion with Surface Topography in the Penn State Pediatric Ventricular Assist Device*. Presented at the Undergraduate Research Exhibition. State College, PA.

?

## **LEADERSHIP AND INVOLVEMENT**

### **Cru (Campus Ministry), President**

*Spring 2016-Present*

- Promoted spiritual growth and community at weekly gatherings and served as a mentor to organization members
- Led worship and prayer team in 2017
- Pioneered a new student leadership structure and led the executive team during the 2018-2019 school year

### **Penn State Dance Marathon (THON), Volunteer**

*Fall 2015-Spring 2019*

- Stood for 46 consecutive hours in THON 2019, the world's largest student-run philanthropy, which raises over \$10 million annually for childhood cancer treatment and research
- Served as a chair and committee member to support planning and execution for Rules and Regulations (2016), Special Events (2017), Donor and Alumni Relations (2018), Family Relations (2018), and Finance (2019)

### **Hugh O'Brien Youth Leadership Program (HOBY), Facilitator**

*2018, 2019*

- Engaged in meaningful discussions, panel sessions, and activities to facilitate the leadership development of high school sophomore ambassadors
- Collaborated with volunteer staff to organize and execute the annual Central PA HOBY Leadership Seminar

### **Club Powerlifting, Team Member**

*Fall 2015-Spring 2016*

- Committed to improving fitness through participation at team practices
- Encouraged team members to achieve personal strength goals

?

## **SKILLS**

- *Clinical:* Patient assessment of general health, vital sign measurements, ECG measurements, airway management, CPR/first aid
- *Laboratory:* Confocal microscopy, environmental scanning electron microscopy, optical profilometry, statistical data analysis
- *Computer:* Microsoft Office (Word, Excel), FIJI, MATLAB, COMSOL, SolidWorks, MetroPro, emsCharts